TOWARD FLUORESCENCE ENHANCEMENT OF DYES IN MESOPOROUS SiO_2 AND ORGANIC FILMS

by

Peter David Haddix

A Thesis Submitted in the Partial Fulfillment
of the Requirements for the Degree of
Masters of Science in Chemistry

Middle Tennessee State University

2014

Thesis Committee

Dr. Andrienne Friedli, Major Professor

Dr. William Robertson, Committee Member

Dr. Dwight Patterson, Committee Member

Acknowledgements

Several faculty and staff member from MTSU along with Vanderbilt University helped contribute to the technical training and research presented here. I would like to thank Joyce Miller from MTSU Interdisciplinary Microanalysis and Imaging Center for help with SEM and TEM images and training. I would also like to thank: Dmitry Koktysh for fluorescence training of solids at the Vanderbilt Institute of Nanoscale Sciences and Engineering; Dr. Dwight Patterson for fluorescence training for samples in solution; Dr. William Robertson for schematic drawings and sample testing on the BSW device; the Weiss research group of the Vanderbilt engineering department helped with the DIPS process; and Matthew Robinson for the synthesis of dyes used in this research. I would like to thank the researchers who came before me and my lab mates: Ja'be Kiri, Peter Cothron, and Matthew Robinson. A special thanks to Dr. Andrienne Friedli for her guidance and knowledge on this project. Last but not least I would like to thank my family and friends for their support through this chapter of my life.

Abstract

Toward Fluorescence Enhancement of Dyes in Mesoporous SiO_2 and Organic Films

Peter Haddix

Large enhancement of spectroscopic signal is common in Raman spectroscopy on metal surfaces (Surface Enhanced Raman Spectroscopy, SERS).[1] However, only a few studies of fluorescence enhancement have been reported on gold surfaces[2, 3] and GaP/SiO_2 multilayers.[4] Photonic band gap multilayers (PBGM) made of quarter wave stacks of alternating SiO_2/TiO_2 layers were designed at MTSU[5] to generate Bloch surface waves (BSWs). The PBGMs were used to observe label-free protein/antibody binding events at the multilayer surface with higher optical sensitivity than for fluorescent dye-labeled proteins and antibodies on glass substrates.[6] Here we report the investigation of enhancement of fluorescence through coupling with BSWs in PBGMs. MATLAB simulations showed that BSWs are maximized inside the PBGM top layer.[7] Three different materials were characterized for optical response on PBGM: m-SiO_2, poly (methyl-methacrylate, PMMA), and AF1600 (Teflon copolymer).

Table of Contents

Page

Tables **Page**

Figures **Page**

CHAPTER I

INTRODUCTION

1.1 Background

Fluorescence sensing is a common practice in the detection of biological and chemical analytes. Through the use of surface enhanced spectroscopy, researchers can narrow in and quantify small amounts of analyte with high sensitivity. Surface enhanced spectroscopy is the technique used to determine the interfacial binding events or adsorption of analyte onto the surface of a material. One of the most common surface enhanced spectroscopies is Surface Enhanced Raman Spectroscopy (SERS). It employs the use of specifically made metal films that have Raman active molecules adsorbed onto the surface. SERS is said to increase the Raman signals 10^7-10^8 fold and can increase it as high as 10^{10} or 10^{12} in optimal conditions.[1]

Fluorescence spectroscopy is another surface enhanced spectroscopic technique that is a sensitive method with the potential to overcome limitations of SERS: portability, cost, and easy operation. Instead of using metal films, photonic band gap multilayers (PBGM), which have been proven to generate Bloch surface waves (BSWs). can be used. BSWs have been observed in materials and are analogous to surface plasmons (SPs) in thin metal films. It is the goal of this research to look for evidence of fluorescence enhancement in PBGMs and to use it as a direct spectroscopic tool for detecting fluorescently labeled species. As a proof of principle, we set out to incorporate fluorescent material into the final, or top, layer of a PBGM with either a mesoporous silicate film or dye doped polymer film and demonstrate the increased fluorescence.

1.2 Fluorescence Testing

1.2.1 Fluorescence

Fluorescence is the process in which a molecule emits a photon after absorbing light at a particular wavelength. The photon emitted is at a longer wavelength which corresponds to lower energy: $E=hc/\lambda$, where E is energy, h is Planck's constant (6.626×10^{-34} m^2kg/s), c is speed of light (3.00×10^8 m/s), and λ is wavelength of the emitted photon.

This equation shows energy and wavelength are inversely proportional to one another giving lower energies at longer wavelengths. Figure 1 below is known as a Jablonski Energy diagram and represents the process of molecules transitioning from the ground state (S_0) to the first and second excited states (S_1 and S_2).

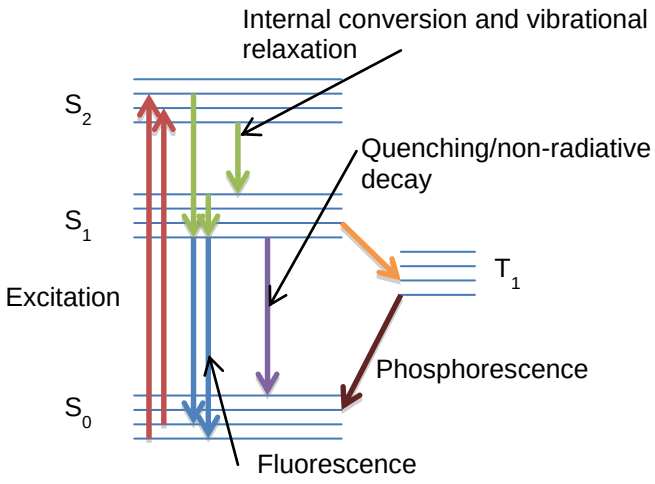

Figure 1. Jablonski energy diagram of fluorescent and phosphorescent excitation, emission, and non-radiative relaxations.

As you can see from Figure 1, once a molecule is excited to a higher energy level it can emit a photon (fluorescent light) and relax back to the ground state. This occurs when the absorbed energy reaches higher vibrational levels of an excited state and rapidly loses excess vibrational energy dropping to the lowest vibrational level of that excited state. Once in the lowest vibrational level of an excited state, S_2 or higher, internal conversion occurs where the molecule transfers from the lowest vibrational energy level of the upper electronic state to the highest level of the lower electronic state that has the same energy. These processes are shown in Figure 1 by the green arrows. The molecule then loses vibrational energy again until it reaches the lowest vibrational level of the first electronic excited state (S_1). From the first excited state the molecules energy can be released in the form of a photon and return to any vibrational level of the ground state (S_0).[8] This is represented by the blue arrows going from S_1 to S_0. Releasing a photon is not the only relaxation pathway the molecule undergoes returning to the ground state. Intersystem crossing can occur resulting in phosphorescence as well as non-radiative relaxation and quenching.[8] Quenching occurs in several different ways and is considered any process resulting in the decrease of fluorescence intensity. Two main types of quenching are dynamic and static. Dynamic quenching occurs in the excited state when fluorophores and quenchers collide. The quencher provides the non-radiative relaxation route from the excited state to the ground state. Static quenching is quenching that occurs in the ground state. This is where the quencher forms a non-fluorescent complex with the fluorophore in the ground state preventing fluorescence from happening. Photobleaching can also be considered a quenching process but is time sensitive. High radiation, such as sunlight,

chemically destroys the fluorophore, resulting in a quenching effect.[9] Keeping the sensor design in mind, if the molecule used to test fluorescence is quenched in any way, the fluorescence intensities or increase in fluorescence yield cannot be properly evaluated. Choosing the right types of dye molecules and other materials for this research was of importance to minimize quenching effects.

Fluorescence spectrometers provide a way to analyze the absorption and emission of light when a molecule is excited by an external energy source. There are five main components of a fluorescence spectrophotometer: light source, excitation monochromater or filter, sample holder, emission monochromater or filter, and detector. The light source excites the molecule into its excited state. The monochromators or filters allow the analyst to set the range of wavelengths that the sample comes in contact with or that it will emit.[8] Data aquisition software is used to convert the data sent to the detector into a spectral format. From the spectra the analyst can determine the excitation and emission wavelengths of a molecule excited at specified wavelengths.

1.2.2 Fluorescent Molecules

Not every molecule that absorbs light or energy will emit a photon. Molecules that do emit photons are known as fluorophores which are very similar to chromorophores. The important characteristic of the molecule is that it has a conjugated π bonding system. This allows for a system of adjacent overlapping p orbitals across a molecule to transfer electrons. A typical cyanine dye which shows an extended π bonding system is shown in Figure 2.

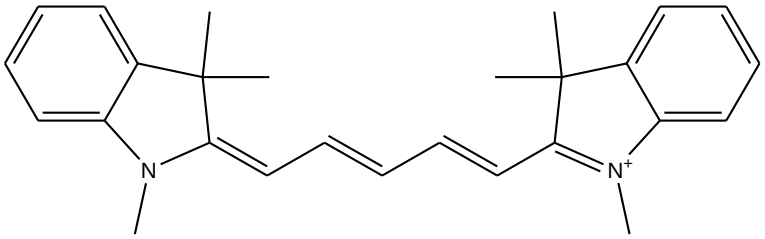

Figure 2. The structure of Cy5, a fluorescent dye commonly used in fluorescence testing.

Figure 2 shows a commonly used fluorescent dye, Cy5, which has a conjugated π system that allows for electrons to transfer from one side of the molecule to another. Other things to consider include the absorption of energy transitioning the molecule from ground to excited states, typically the n - π* and π - π* transitions. Figure 3 represents these electronic transitions.

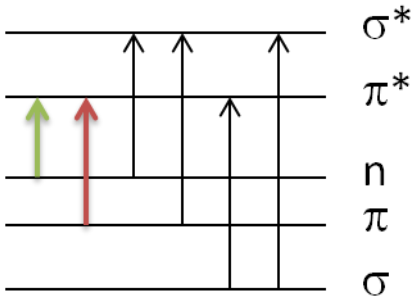

Figure 3. Electronic transition states focusing on the n – π* (green arrow) and π – π* (red arrow)

The absorption band corresponding to n - π* transitions (Figure 3, green arrow) commonly have small extinction coefficients leading to long lifetimes. This transition usually has a small quantum yield and is dominated by nonradiative relaxation. The π - π* transition (Figure 3, red line) usually has a high extinction coefficient leading to a shorter lifetime. Molecules exhibiting this type of transition are more likely to fluoresce.[9]

1.2.3 Fluorescent Polymers in Sensing

This project aims to demonstrate an increase in fluorescent yield and its application in a sensing device. Fluorescent polymers (FPs), or conjugated polymers, can be used in fluorescence sensing in one of two ways: amplification of the fluorescent yield or quenching of fluorescence. The latter is the more commonly used application. This is due to polymers acting as electron donors that have delocalized electronic excited states that can travel quickly though the conjugated polymer increasing the interaction with a quencher.[10,11] A common sensing application for FPs is the detection of nitroaromatic, nitramine, and nitrate ester explosives. Nitroaromatic compounds are used as quenchers because of their electron accepting capabilities. The nitroaromatic compounds (NACs) can act as an electron acceptor for the excited electrons of a FP in redox sensing. This concept is illustrated in Figure 3 and is a dynamic quenching system.

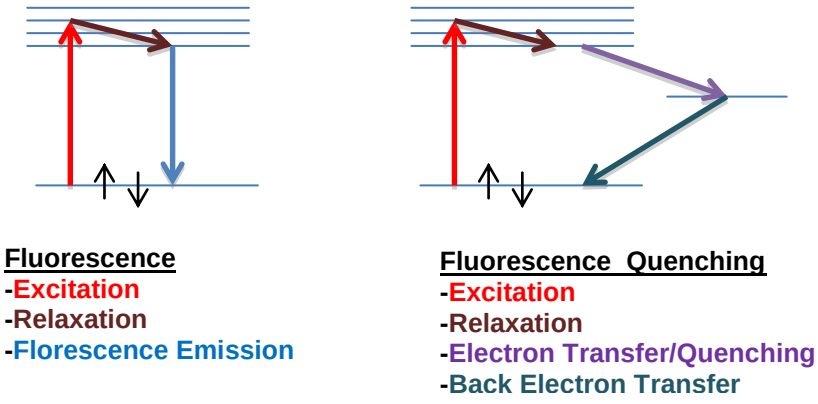

Figure 4. Quenching mechanism of electron accepting NACs[10,11]

Figure 4 shows that when the electrons are transferred from the excited polymer to the electron acceptor, the electron is then transferred back to the ground state of the polymer molecule in turn quenching the fluorescence of the polymer.[11] Toal *et al* have reported detection limits of these explosive compounds down to parts per trillion.[11]

Another application for FPs is in sensing biological materials. Chen *et al*[10] reported a greater than million-fold amplification in fluorescence quenching with a polyanionic conjugated polymer poly(2-methoxy-5-propyloxy sulfonate phenylene vinylene) (MPS-PPV). In a dilute solution the MPS-PPV acts like *trans*-stilbene and its derivatives. *Trans*-stilbene is known to be quenched by electron deficient aromatic compounds similar to the NACs discussed previously. *N*, *N*'-dimethyl-4-4'-bipyridinium (MV^{2+}) is used as the quencher in Chen *et al*'s study. An equation relating a constant K_{SV} to the concentration of MV^{2+} was used to determine the quenching sensitivity: $\phi^0 / \phi = 1 + K_{SV} [MV^{2+}]$. This is the Stern-Volmer equation for dynamic quenching where

ϕ^0 and ϕ are quantum efficiencies of fluorescence in the absence and presence of MV^{2+}, and $[MV^{2+}]$ is the concentration of the quencher.[9,10]

In the study it was shown that the K_{SV} value for t*rans*-stilbene and MV^{2+} in a homogeneous solution was $K_{SV} = 15$. When testing *trans*-stilbene as a micelle the K_{SV} value increased to $K_{SV} = 2 \times 10^3$. The quenching constant for MPS-PPV in dilute solution produced a value of $K_{SV} = 1.7 \times 10^7$. This K_{SV} value is six orders of magnitude larger than the dilute stilbene solution. With increased quenching sensitivity, the MPS-PVV polymer was prepared on a glass slide to test solid state fluorescence when in the presence of dinitrotoluene (DNT). By fluorescence quenching, the thin film detected DNT at a level of $< 8 \times 10^{-9}$ M.[10]

1.2.4 Doped Fluorescent Materials

Doping a material with a fluorophore is a common way to introduce fluorescent molecules into other materials at controlled concentrations. Vu *et al* and researchers explored the use of pyrene derivatives, as a fluorophores to dope mesoporous silica films and test quenching performance in the presence of NACs. They used a donor-substituted pyrene to synthesize 1,3,6,8-tetrakis-(4-methoxyphenyl)pyrene (TKMPP) to act as the fluorophore in mesoporous silica thin films. Thin films of different mesostructures were prepared by spin-coating mixtures of TEOS, P123 surfactant, and TKMPP in a mixture of ethanol and tetrahydrofuran on quartz substrates. The P123 surfactant was removed after the film had cured at 100 °C for 24 h by calcining the film at 450 °C for 6 h. Gas sensing experiments showed that when the mesoporous thin films were exposed to NACs, the

fluorescence of the doped films was quenched. It was reported that the doped thin films with wormlike mesopores were efficiently quenched in the presence of DNT with detection limits on the order of 10^{-8} M.[12]

Additionally, dye doped polymers have been used in the enhancement of fluorescent signals. Creating fluorophore-doped polymer thin films can increase the fluorescence of the fluorophore when applied to the right substrates. Coumarin 460 in chlorobenzene mixed with a 2 % polymethylmethacrylate to create a 20 mM solution fluoresced in the UV region at 460 nm. Three different substrates were used for comparison; bare quartz slides, gold, and silver thin films. The gold and silver films are surface plasmon generating materials which are responsible for the increase in fluorescent yield. An 11-fold increase from bare quartz to silver films was observed.[3] Materials generating surface plasmons and other surface electromagnetic waves, as well as their importance will be discussed in further detail in the following sections.

1.2.5 Fluorescent Labels

Fluorescent labels are fluorophores derivatized with reactive functional groups that are bound to other molecules. Common molecules used as labels include peptides, nucleic acids, proteins, and other biological molecules. Using fluorescent labels is a common practice for detection in the bioanalytical field.

1.3 Photonic Band Gap Material

Fluorescence enhancement can be seen in fluorescence spectroscopy by employing the use of surface plasmons. Thin metal films generate a SP along the surface of a conductor, metal, dielectric non-conducting material. The general idea behind the SP

is that light is trapped on the surface of the metal through interactions with the free electrons of the conductor. The free electrons of the conductor oscillate collectively in resonance with the light wave. The interaction between the oscillating surface charge and the electromagnetic field of the light generates the SP and its intriguing properties.[13] Figure 5 shows the interaction between the electromagnetic field and surface charge.

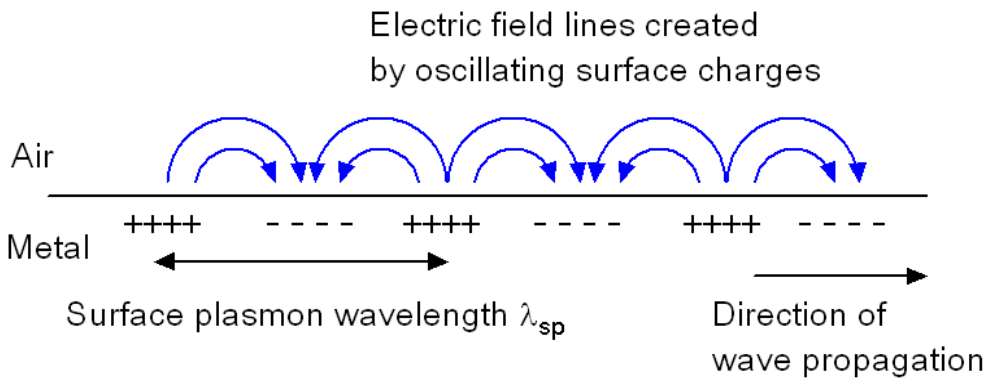

Figure 5. SP generation from electromagnetic waves coupling with oscillating free electrons of dielectric surface between air and metal interface.

The electromagnetic field associated with SPs exponentially decay as a function of distance from the surface of the metal. This means that all the enhancement from the coupling is generated at or near the surface of the interacting species.[13] The sensing apparatus that takes advantage of SPs can be used as a label-free device due to the fact that the sensing takes places with changes at the surface of a metal film with interacting species. A mode occurs when a light source is coupled to the SP of a thin film and absorbed so that little or no reflected light is captured by the photodetector. When the

angle of incoming light needed to produce a mode is changed it is said to be a mode shift. A mode is observed before the interaction takes place. Once the species of interest is bound to the metal surface a shift in the mode is observed.[5] Reflectivity dips, or modes, for three idealized materials were calculated and are shown in Figure 6.

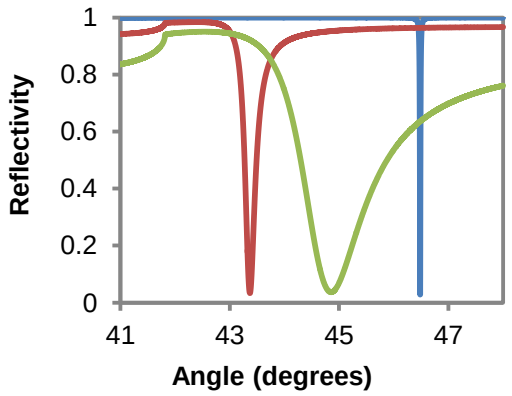

Figure 6. Calculated total internal reflectance, or mode, shown for silver (red), gold (green), and photonic band gap multilayer (blue) substrates.

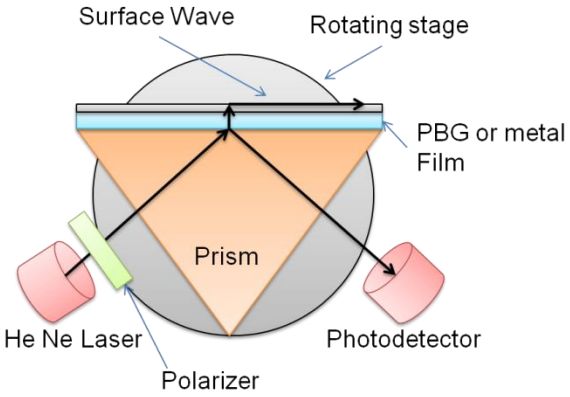

Figure 7. Sensing apparatus used in SP and BSW sensing

A photonic band gap (PBG) is a region where the emission of photons is forbidden. Using a PBG multilayer (PBGM) in the sensing apparatus allows for light to be emitted in this forbidden range.[5] A BSW is analogous to a SP in a thin metal film but takes place on the surface of a PBGM. The PBGM is engineered to have effective optical properties like a thin metal film and is comprised of alternating layers of high and low refractive index materials. For this research the alternating layers are TiO_2 (high refractive index) and SiO_2 (low refractive index). The PBGM is 12 alternating layers of TiO_2 and SiO_2, with TiO_2 layer on the bottom, or at the prism PBGM interface, and the final layer is SiO_2. Using these two materials with the appropriate thicknesses allows the PBGM to act like a thin metal film at any desired wavelength.[5] Another advantage of the PBGM is that it has a very low dielectric loss. The dielectric loss of periodic stacks of non-metal components is orders of magnitude lower than the lowest dielectric loss metal.[5] These advantages make the PBGM a superior material in sensing compared to the thin metal films commonly used.

1.3.1 Fluorescence Enhancement

Liebermann *et al* discussed field enhanced fluorescence spectroscopy based on surface plasmon interactions.[2] The research exploited the fact that surface plasmon spectroscopy allows for label free detection of binding events. Fluorescent molecules are used to increase the signal of the binding events of the sensing apparatus, especially when the analyte is in low concentration or of low molecular weight.[2] A helium neon (HeNe) laser was used as the light source and a set up similar to that in Figure 6, except the addition of a flow cell to pass solutions over a thin metal film. The research was

concerned with sensing the binding of streptavidin molecules with a biotin derivatized fluorescent dye. It was discovered that a fluorophore needed to be within certain proximity of the SP enhanced field to show good fluorescence enhancement. This distance is known as a Förster radius. Within one Förster radius (5-7 nm) the fluorescence is quenched by dissipating excitation energy into the Au film as heat. Slightly further away from this radius, fluorescence is seen but some of the excited light is coupled back to the metal. This in turn excites SP and the SP mode re-radiates through the prism. Outside of this range but still within the evanescent tail of the SP, normal fluorescent decay occurred.[2] This was demonstrated by creating multilayers on the surface of an Au film. The first layer was a binary thiol mixture containing biotinylated thiol and OH-terminated diluent thiol. This was followed by a streptavidin monolayer created by specific binding of streptavidin to biotin sites on the surface of the film. Biotin labeled latex particles, which were fluorophore doped, were rinsed through the cuvette to bind to the streptavidin monolayer. A clear angular shift in the SP reflectivity was seen with the binding of the latex beads with a fluorescence enhancement of 15 fold and a multilayer thickness of 142 nm. Another test was run by attaching a biotinylated fluorescent dye (BFD) to the streptavidin monolayer. The angular reflectivity was measured for the attachment of each layer in this experiment. With the addition of each layer an angular shift was seen except for the addition of the BFD binding. The resulting fluorescence measured in parallel with each binding layer did show a SP field enhanced excitation when the BFD was attached. The emission intensity was not intense as the latex particle test above because the BFD layer is much smaller, about a 5 nm multilayer

thickness, leading to non-radiative decay as heat back into the Au film.[2] While these experiments showed that SP can be used for fluorescence-enhanced label free sensing in the presence of surface plasmons, the fluorescence enhancement needs to be improved.

Fluorescence enhancement through the use of photonic crystals (PC) has been proven in the past.[14,15] The PC can overcome some of the problems that arise from SP spectroscopy. For example, the fluorophore attached to a PBGM does not need to be as far away as when attached to a SP generating material. The distance is less critical because of an absence of quenching and strong absorption effects caused by the thin metal films. Also, signal loss is not a problem because the enhancing medium is made of dielectrics in BSW analysis.[16]

BSW on multilayer PBG materials , PBGM, has become a common concept in sensing applications since the MTSU research PBGM began.[4,16-18]

PCs on glass substrates were created by using a vertical deposition method with a suspension of poly(styrene-methylmethacrylate-acetic acid)[15] and were used to test solid state fluorescence enhancement of organic dyes. Rhodamine B (RB) base, coumarin, and tris-(8-hydroxyquinoline) aluminum (AlQ_3) were each deposited (under vacuum) on the PC and aluminum films for comparison. A 20-fold enhancement of fluorescence in the PC film, as compared to the Al film, was seen for RB when deposited on a yellow PC surface. Coumarin and AlQ_3 were deposited on cyan and green PC films with an enhancement of 14 and 9 fold.[15] The dye molecules were deposited on different color PC so the excitation or emission wavelengths of the excited dye were in the range of the photonic band gap of the matching PC.

Research done by Gao *et al* has experimentally demonstrated fluorescence enhancement of 50 to 69 fold using an alternating PBGM of gallium phosphide (GaP) and silicon dioxide (SiO_2) multilayer.[4] A three period (pairs of layers) structure with GaP as the high refractive index and SiO_2 as the low refractive index material, were made using a RF magnetron sputtering method.[4] The set up to test the fluorescence is a Kretschmann configuration similar to that in Figure 6 with the aid of a HeNe laser. The fluorescing material, carboxylated quantum dots, was spin-coated onto the PBGM surface.[4] These materials were compared to regular glass slides. Both S and P polarized light were used resulting in a fluorescence enhancement of 50 fold for S polarized light with a 3 period 1D PBGM and 69 fold for P polarized light with a 3.5 period 1D PBGM.[4] S-polarized light refers to the electronic field of light traveling perpendicular to the line of incidence while P-polarized light is the electric field traveling parallel to the line of incidence.[19]

1.3.2 Wave Guides

BSW are surface electromagnetic waves that propagate along the air interface of a properly engineered PBGM. BSWs cannot be excited directly with incident light because of a mismatch between the wavelengths of light in air and the BSW at a given frequency. A prism can be used to shorten the wavelength of the laser light in order to couple the light with the BSW. Converting the incident laser beam into a narrowly confined BSW increases the electromagnetic field strength at the surface. This increase is demonstrated in Figure 8.

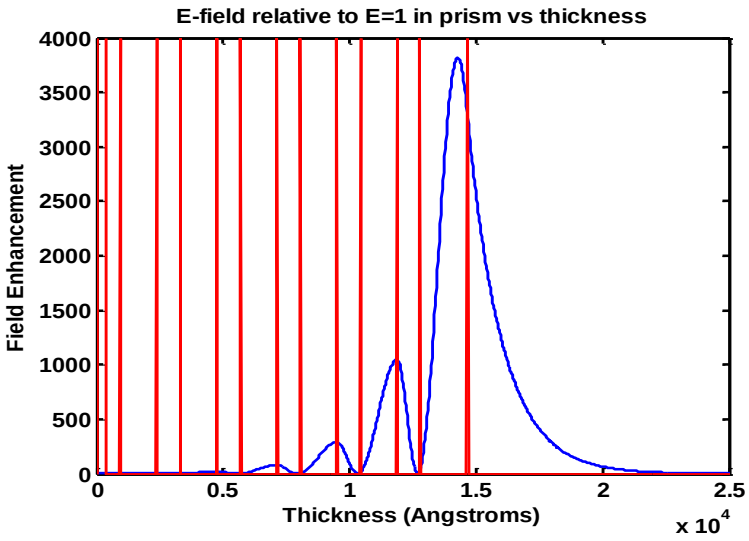

Figure 8. Wave propagation through TiO_2/SiO_2 PBGM

If a grating is used to couple the incident light to the BSW the same increase in electromagnetic field strength will still occur. The grating can replace the prism in the sensing apparatus because it diffracts light in a way that allows wavelength matching between the light from the HeNe laser and the BSW. As light passes through the material it will be diffracted away from the surface as well as diffracted parallel or into the surface. The light that is diffracted into the surface can then couple to the BSW eliminating the need for a prism. Researchers in MTSU's Department of Physics and Astronomy are calculating the right grating needed for such a coupling method to work.

Multilayers have become common applications in sensing devices.[20] BSW controlled fluorescence enhancement of dye labeled proteins has been seen by Descrovi *et al* and their research has advanced to show this effect in a polymer waveguide on a one dimensional photonic crystal.[21]

1.4 Sensing Apparatus

A label free detector was developed based on the techniques and concepts discussed in Sections 1.2 and 1.3. The material used as the sensor is a PBGM constructed of 12 alternating layers of TiO_2, a high refractive index material, and SiO_2, a low refractive index material on quartz slides. COMSOL and MatLab calculations showed that field enhancement is maximized in the final layer (SiO_2) of the PBGM.[7] A computer generated model of this maximum is shown in Figure 8. Figure 8 shows the increase in electromagnetic field strength in the final layer (SiO_2 layer) of the PBGM. It is this layer that the applied m-SiO_2 or polymer thin film will be added so that the maximized field strength will take place in the modified thin film. With an increase of almost 4000 in the field intensity, the energy on the surface will allow for the increase in fluorescent emission by acting as the excitation energy source.

The sensing apparatus to test fluorescence and mode shifts is shown in Figure 6. The laser is a HeNe laser that operates at 632 nm. The laser light is S-polarized, parallel to the surface of the film, and is incident on the multilayer through a prism (refractive index of n = 1.52) on a rotation stage. The rotation stage is used to scan the angles of reflectance and determine the angle of incidence at which light couples to the BSW mode. Films with gratings applied can be tested with the same apparatus with the prism removed. Proving this concept will allow for the simplification of the sensing device and further the benefits of the sensing apparatus.

1.5 Research Objective

The goal of this research was to synthesize thin films to act as the terminating layer of a PBGM and determine the fluorescence limitations of dyes applied to these thin films. This was done by engineering a PBGM with only a partial final layer (SiO_2 layer) allowing for any material to be used to complete the PBGM. Thin films can be applied to the PBGM where the field enhancement exists (Figure 8) and couple to BSW generated by the photonic band gap. This final layer approach has not yet been investigated for sensing applications with a SiO_2/TiO_2 PBGM. Two thin films were generated to act as the completing layer of the PBGM: mesoporous silicon dioxide, and dye doped amorphous polymers. Mesoporous silica films are used in abundance for sensing applications.[22] These films allow for a high loading of analyte due to the increased surface area of the material. Mesoporous silicate is easily functionalized, which allowed for a fluorophore functionalized mesoporous films for fluorescence testing. The polymer thin films used in fluorescence testing were dye doped amorphous polymers. The fluorescence limitations will be found to help calibrate the sensing device before fluorescence comparisons are made on the PBG. With the application of these materials we hope to demonstrate a label free sensing device that will also show an increase in fluorescent sensing capabilities.

CHAPTER II

MESOPOROUS THIN FILMS

2.1 Materials

Pluronic® F-127 (F127) purchased from Sigma Life Sciences. Ethyl Alcohol (EtOH) (200 proof, ACS/USP grade) purchased from Pharmco-AAPER. Silica wafers (50.8 mm diameter, 250-350 um thickness, single side polished) were purchased from Wafer World, Inc. Toluene (99.8% anhydrous) and tetraethyleorthosilicate (TEOS) were purchased from Sigma Aldrich. 3-Aminopropyl-triethoxysilane (APTES) was purchased from Acros Organics. Hydrochloric acid (12.1 M) was purchased from EMD Chemical. Fused silica slides (2x2 in) were purchased from Dell Optics. The photonic band gap multilayers (PBGM) were designed by Dr. William Robertson (MTSU Physics and Astronomy Department) using Matlab[7] and manufactured at Thin Film Laboratories, Milford, Pennsylvania.

2.2 Thin Film Synthesis

2.2.1 Sol-Gel Synthesis

Sol-gel syntheses used variations of a literature recipe.[23] F127 (2.00 g) was dissolved in EtOH (13.0 mL) in a 50 mL round bottom flask. TEOS (4.6 mL) and H_2O (0.8 mL) were then added, followed by 2 M HCl (0.122 mL) and the solution heated at reflux for 1 h. The solution with a molar composition is TEOS-F127-H_2O-HCl-EtOH = 1: 7.30 x 10^{-3}: 2.03: 0.011: 10.2.

The acid-catalyzed synthesis of the SiO_2 sol-gel was used to create films of varying thicknesses and porosity. Removing the F127 from the recipe allowed for non-

porous films to be formed. Varying the amount of solvent (EtOH) gave control over thickness of films; more solvent gave thinner films while less solvent created thicker films. Spin-coating multiple layers of films, mesoporous films on top of non-porous films, was also performed to create thicker films with a mesoporous final layer.

2.2.2 Thin Film Formation

After sitting over night, the sol-gel (60 µL) was spin-coated onto silicon wafers with a P6000 Spin Coater for 30 s at 2000 rpm and dried in a high humidity atmosphere (desiccator with petri dish containing water in the bottom) to slow the drying process. Films were then calcined in a programmable Lindberg quartz tube furnace to burn off any organic materials, leaving behind a mesoporous (m-SiO_2) thin film. The furnace was programmed to heat the m-SiO_2 samples at a rate of 1 °C / min from room temperature to 400 °C, held for 1 h, ramped again to 600 °C at 1 °C / min and held for 1 h. The program for the calcination of PBGM was altered due to the nature of the substrate. The spin-coated non-porous SiO_2 films on PBGM were calcined at a ramp rate from room temperature to 400 °C at 1 °C / min and held for 1 h then brought down to 25 °C by 1 °C / min. Another calcination program was run from 25 °C by 1 °C / min to 200 °C, held for 2 h, cooled to 25 °C at 1 °C / min, and then F127 extracted in methanol (MeOH) for 4 h. Extraction for 24 h gave the same results when TEM images of each material were compared.

2.2.3 APTES Coating

All procedures using APTES were performed in a glove box (Labconco) in an Ar atmosphere dried with $CaCO_3$ (Drierite) to eliminate excess water. A 1% v/v solution of APTES in anhydrous toluene was used to coat samples in for 1 h. The samples were then rinsed in a beaker, placed in a staining jar, and covered with toluene. The jar was removed from the glove box, samples dried under stream of N_2 gas, and then placed on a hot plate (110 °C) to remove excess toluene and complete the coating process.

2.2.4 Cy5 Synthesis

A stock solution of Cy5-NHS ester ($3.2x10^{-4}$ M) was created by diluting Cy5 (1.2 mg) with EtOH (1.0 mL). Portions of the stock solution (10 μL) were then diluted with EtOH to create 10:100, 10:1000, and 10:10000 sample solutions.

An EtOH-saturated environment was created by placing an evaporating dish with EtOH (12 mL) in the bottom of an empty dessicator, covered, and left for 1 h. APTES-coated mesoporous thin films were then placed in the dessicator and Cy5 sample solutions (10 μL) were added to the films, dessicator covered, and left to sit for 1 h. The mesoporous films were then placed on glass slides on a hotplate at 90 ^{0}C for 1 h. The films were then placed in a staining jar full of EtOH for 5 min. and dried under a high purity N_2 stream. The washing and drying process was then repeated.[24]

2.3 Measurement Methods

2.3.1 Transmission Electron Microscopy (TEM)

TEM uses a magnetically focused high voltage beam of electrons that travels in a vacuum through a sample. Depending on the composition of the sample, some of the electrons are scattered and lost while the rest travel through the sample to give an image.[25] A charged coupled device (CCD) camera is placed in the path of the electron beam to capture a digital image of the sample. The TEM can produce an image up to 1,000,000x magnification and a resolution below 1 nm. Objects not seen by typical microscopes can be seen from a 1 μm to 1 nm scale range. This means that the TEM can be used to analyze samples on the sub-micron level. This gives the TEM a variety of applications in the biological, medical, and materials science fields.[26] Sample preparation was done by scraping films, with a scalpel tip, off silicon wafers and onto Formvar-coated copper slides with a grid layout on them. The thin films were analyzed using a Hitachi H-7650 Transmission Electron Microscope, Japan, set to high voltage (100.0 kV). Once the images of the films were taken, the pore size was analyzed by ImageJ. The scale of the image was set to the scale bar given on the image produced by the TEM imaging software. Once the scale was set, straight line measurements were taken across the width of the pores to give the diameter.[27] Histograms were created in Excel using the data from ImageJ to determine the average pore size in the thin films.

2.3.2 Profilometry

Profilometry is a surface analysis technique that is used to quantify roughness of a materials surface. It uses a diamond-tipped stylus to measure the differences in surface structures.[28] To measure the thickness of the films a piece of tungsten wire is used to score the films to remove any film from the scoring mark while leaving behind the intact substrate. This allows the machine to calculate the difference in height between the film and the scored mark, where there is no film, with sensitivity down to 1 angstrom. The film thicknesses were determined using a KLA Tencor P-16^{+} Profilometer; Milpitas, California. The edges of the films are much thinner than the middle due to the spin-coating process, so the measurements were averaged together across the film surface. The scanning parameters were: length, 240 μm; sampling rate, 50 Hz; speed, 50 μm/s; scan time, 4.8 s; total data points, 241; applied force by stylus, 2.00 mg; stylus radius, 2.00 μm.

2.3.3 Ellipsometry

Ellipsometry is a measurement technique that uses polarized light to measure microstructures of thin films, surfaces, and other materials. The ellipsometer detects the change in the polarization of light reflected from, or transmitted through, the sample back to the instrument. Two of the most common applications are the characterization of thin film thickness and determination of optical constants. Other applications include; alloy ratio, crystallinity, depth profile of material properties, and growth or etch rate (in-situ).[29]

The ellipsometer used was a J. A. Woollam M-44 Spectroscopic Ellipsometer, USA, with a LPS-400 75W Xenon Light Source and an EC-270 Electronics Control Module. The data acquisition and analysis program used was WVASE32 run by Windows 95. The ellipsometer was initialized at a 70° incidence angle. The model layer for the data acquisition was: Si.mat with a 1mm set thickness as 0 layer; layer 1 was cauchy.mat with a fit thickness estimated at 200.0 nm.

2.4 Mesoporous Results and Discussion

The original goal of the m-SiO_2 thin film was to create a 1 μm thick film to replace the final SiO_2 layer of a PBGM (PBGM-1). PBGM-1 was engineered so that a film of this thickness would produce a mode when analyzed with the HeNe laser. A mode is given when the light from the HeNe laser is coupled with the BSW created by the material. This can be seen by the naked eye because at this specific angle no light will be reflected back through the prism in the Kretschmann configuration. A white sheet of paper is placed where the light reflects back to the desktop to aid this process. When viewing the scattered light on the sheet of paper it is possible to see a horizontal line with no scattered light. It is at this angle that the light from the laser is being coupled to the BSW of the PBGM.

The films were made by reducing the amount of solvent (EtOH) used in the sol-gel synthesis of the original film (M).[23] Two thicker films were created by removing 30% of EtOH (M_1) and 20% of EtOH (M_2) form the sol-gel synthesis. Since it was necessary to completely replace the final layer of the PBGM-1, and in some cases this was not

possible with just the m-SiO_2, solid layers of SiO_2 (S_1 and S_2) were synthesized. The m-SiO_2 films could not produce desired thickness due to cracks and fractures in the material. The solid films were created by removing the tri-block copolymer, F127, from the sol-gel synthesis. In the SiO_2 film synthesis the same amount of EtOH was used as in the m-SiO_2 synthesis (S_2 corresponding to M_2). Without the F127, calcining the films gave a non-porous thin film that could support a porous film when layers were spin-coated one on top of the other. The thickness of films made by this stacking process and removal of solvent can be seen in Table 1.

Upon further investigation, a newly engineered multilayer, PBGM-2, allowed for a m-SiO_2 film to be as thin as possible. This called for a new approach in synthesizing the m-SiO_2. PBGM-2 was engineered so only part of the final SiO_2 layer was missing. This is why the films needed to be thinner because now the m-SiO_2 was only replacing a partial layer of SiO_2 on the PBGM. EtOH was added to the sol-gel synthesis after the 1 h reflux in hopes of creating the thinner films. Increasing the EtOH by 200% (M_3) and 262% (M_4) created these thinner films. The thickness of these films is also found in Table 1.

Table 1. Thin Film Thicknesses

	Film Thickness (nm)			**Average (nm)**
M	714	749	793	752
M_1	748	744	729	740
S_1M_1	795	791	788	791
M_2	792	1200	1500	1164
S_2M_2	1400	1457	1435	1431
$S_2S_2M_2$	2400	1800	2000	2067
M_3	519	516	565	533
M_4	281	330	362	324

Table 1 shows the average thickness of M_2, S_2M_2, and $S_2S_2M_2$ are all thick enough to be used as the final layer of PBGM-1 but never showed a mode when analyzed with the HeNe laser. This was due to the fact that the thickness of the films caused cracking on the surface when calcined because the coefficients of expansion of the different materials could not withstand the stress the heating program. These cracks were apparent when determining the thickness of the films by profilometry and could be seen by the naked eye. For the thin films to give a mode they need a smooth surface and good

optical quality. With the cracking on the surface of the films, and possibly throughout the layers, it made it impossible to use them.

The M_4 film had an average thickness of 324 nm and a smooth surface. This film was used as the mesoporous layer on PBGM-2. While no mode was seen on this film, the optical quality of the film was much better than previous films. To increase the desired smooth surface, M_4 films were spun on the spin-coater at the maximum acceleration giving a smoother surface at an average film thickness of 267.7 nm.

A problem occurred during the calcining process for creating the M_4 film. When running the temperature program used for calcination, the films appeared to be cracking or peeling off the PBGM-2 as well as the PBGM-2 peeling of the quartz substrate. We concluded that the difference in the coefficients of expansion of the two materials, TiO_2 / SiO_2 layers of the PBGM-2 caused the cracking.[30] This problem was not observed with the previous PBGM-1 and the thicker films. After several attempts to find the maximum temperature PBGM-2 can reach before deformation, it was determined that PBGM-2 could withstand 200 ºC for 2 h. This thermal treatment will remove water and EtOH from the film leaving behind the F127 template. To remove the F127 and give the desired mesoporous structure, the films were extracted with MeOH for 4 h, as mentioned in section 2.2. Films extracted for 24 h gave the same results when analyzed by TEM.

The film porosity and morphology was determined by transmission electron microscopy and ImageJ analysis. Figure 1 below shows the comparison of the films made by removing EtOH from the sol-gel synthesis (A, B) to thinner films created by adding EtOH to the synthesis (C).

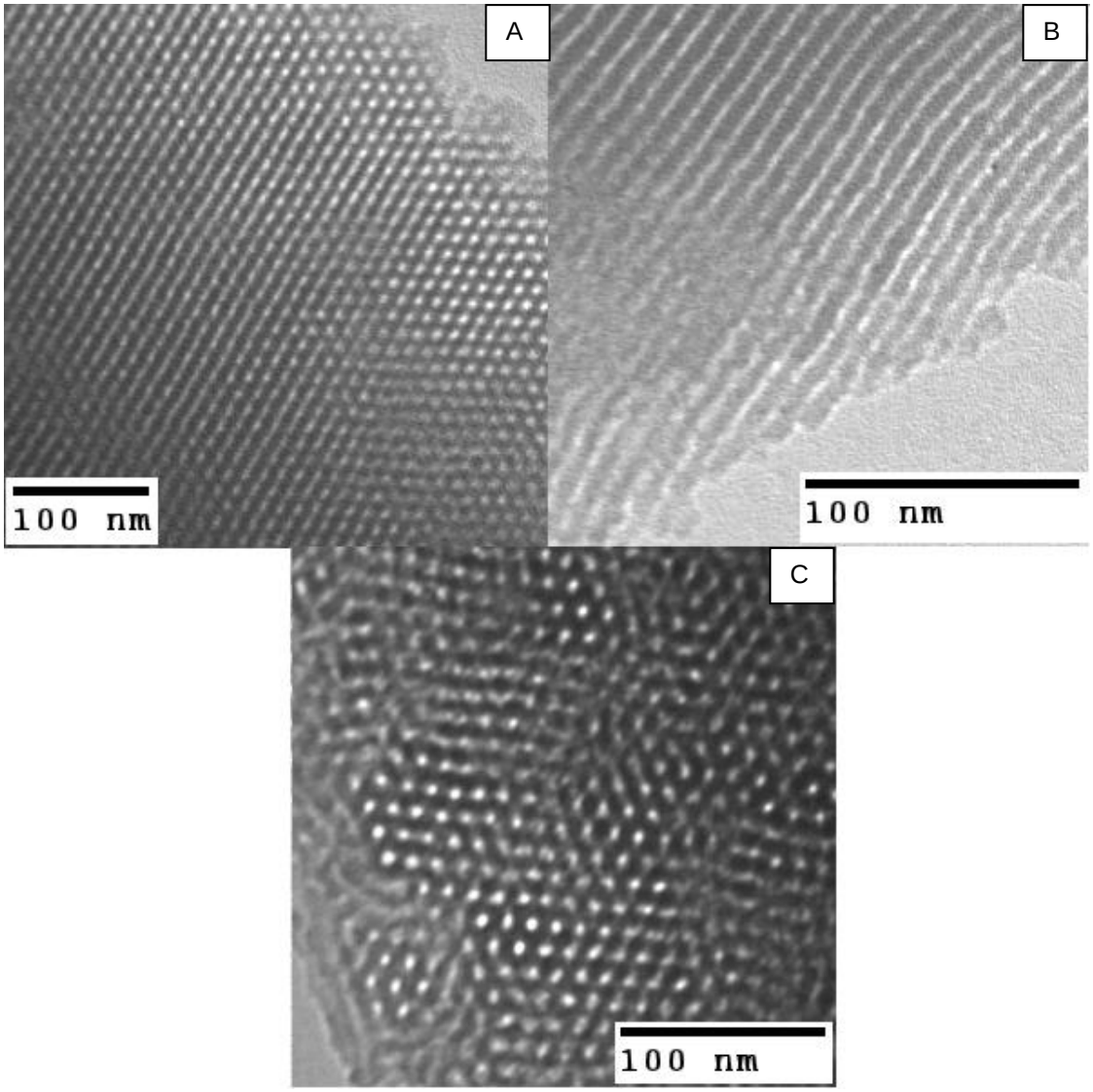

Figure 9. TEM images of thicker film M_1 with hexagonal pore structure (A and B) and the thinner film M_4 with a worm-like mesostructure (C).

The well-ordered mesopores in Figure 9A and Figure 9B show hexagonal pore structures. Figure 9A shows the top view of the hexagonal pores formed from the F127 tri-block polymer. The parallel lines shown in Figure 9B are the pores packed together in a cross sectional view of the film. Figure 9C shows wormlike mesopores that appear abundant but do not have the tightly-packed structure of the hexagonal pores. The change in pore structure is due to the fact that more EtOH was added to the sol-gel after the 1 h reflux. The dilution of micelles in the sol-gel created the different structure of mesopore after F127 extraction. The mesopores are well defined in both hexagonal and wormlike morphologies leading to the expectation that they will both work in the sensing application. Figure 10 shows histrogram plots of the M_4 film that, even though no mode has been seen by the naked eye, gave the best optical quality film. The average pore size was determined for M_4 by measuring 50 random pore diameters from 5 different TEM images. The average overall pore diameter was determined to be 7.0 nm. Histograms were created to determine the most often occurring mesopore pore diameter (Figure 10). Figure 10 shows that the most abundant pore diameter in the mesoporous structure of M_4 to be 6.32 nm and a range of pore diameters from 3.43 nm to over 9.22 nm. This plot was generated in Microsoft Excel by using the histogram function. With pore sizes in this range it is possible for the m-SiO_2 to be used in a wide variety of sensing applications.

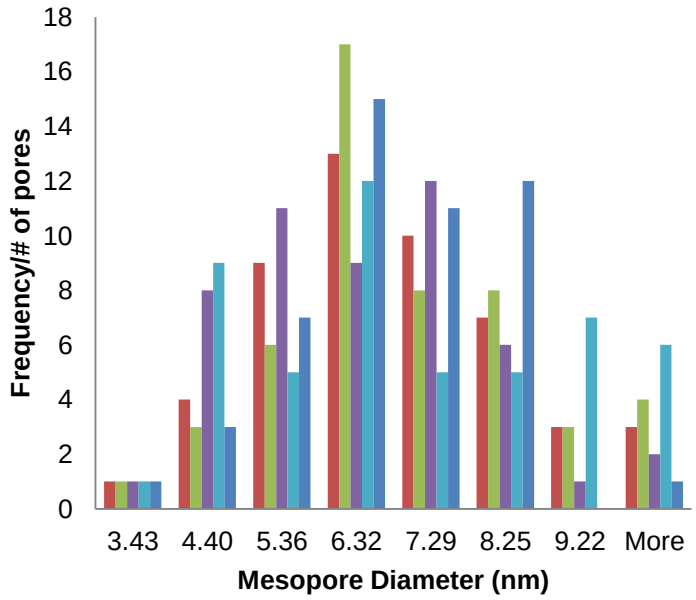

Figure 10. Histogram plot showing the frequency of mesopore pore diameters from the 5 TEM images used to find the average pore diameter discussed above.

CHAPTER III

POLYMERS AND FLUORESCENCE

3.1 Materials

Octafluorotoluene and poly [4, 5-difluoro-2, 2-bis (trifluoromethyl)-1, 3-dioxole-co-tetrafluoroethylene] (AF 1600) (65 mol % dioxole) were purchased from Sigma Aldrich. Chloroform (99.8%, spectroscopic grade, stabilized) was purchased from Acros Organics. Poly(methyl methacrylate) (polydispersity: 2; atactic from free radical polymerization) was purchased for Scientific Polymer Products Inc. Fused silica slides (2" x 2" in) were purchased from Dell Optics. The photonic band gap multilayers (PBGM) were designed by Dr. William Robertson (MTSU Physics and Astronomy Department) using Matlab[7] and manufactured at Thin Film Laboratories, Milford Pennsylvania. Fluorescent dyes **1-7** were synthesized at MTSU by the Friedli research group.[31,32] Cy5 NHS Ester was, dye **8**, was purchased from Jackson Scientific.

3.2 Polymer Film Formation

3.2.1 Polymer Solution

Solutions of amorphous Teflon (AF) 1600 were made at 3, 1, and 0.1 % (w/w) solutions in octafluorotoluene (OFT). In order to obtain a homogeneous solution, AF 1600 was ground with a mortar and pestle before being weighed and the mixture of OFT and AF 1600 was sonicated for 1 h to promote dissolution of AF 1600, not just swelling. A stock solution of 1 % AF 1600 with DMA-2-TB (dye 1) was used to create fluorescent films at varying concentrations.

Poly (methyl methacrylate) thin films were made from 2 % (w/w) solution in chloroform. A 2% (w/w) solution of PMMA with dye **1** in chloroform was also made for fluorescent films at varying concentrations.

3.2.2 Film Formation

AF 1600 polymer solutions were spin-coated with a P6000 Spin Coater onto SiO_2 plates (100 μL) at 2000 rpm for 30 s and dried overnight in covered containers. PMMA solutions were spin-coated (60 μL) at 2000 rpm for 30 s and dried over night in a laminar flow hood. This process was repeated for PGBM slides for both polymer films. AF 1600 and PMMA films with and without fluorescent dye were also made by dropping the solution on the surface of substrates by pipette. The substrates were then covered, and films dried overnight with no spin-coating.

3.3 Dye Preparation

Several dye solutions were tested by UV spectroscopy and fluorescence spectroscopy. These dyes were synthesized by the Friedli research group in MTSU laboratories.[31,32] Stock solutions were made by diluting each dye (2.00 mg) with chloroform (100 mL) and samples made from aliquots of those stock solutions.

3.4 Measurement Methods

Profilometry, Ellipsometry, and TEM were the primary methods of analysis. These were discussed in Chapter II, 2.3.1 - 2.3.3, and will not be repeated in this section.

3.4.1 Fluorescence Spectroscopy

Fluorescence spectroscopy is a technique used in measuring the excitation and emission wavelengths of light given off when electrons of certain molecules are excited

from one electronic state (S_0) to a higher electronic state (S_1). This process is described in more detail in Chapter 1. The excitation and emission spectra of the Cy5 reacted mesoporous silica and fluorescent polymer thin films were measured using Fluorolog-3 FL3-111 Spectrophotofluorometer manufactured by Horiba Jovin Yvon Inc. (Edison, New Jersey). The spectral analysis program connected to the spectrophotofluorometer was FluorEssence version 2.5.2.0. The samples were placed in the solid sample holder with the lamp set for the UV-Visible setting.

For Cy5 samples: excitation wavelength set from 600-640 nm and emission wavelength set from 650-700 nm. For dye **1** doped AF 1600 films the excitation wavelength was set from 375-680 nm with an emission wavelength set at 690 nm. Emission spectra were obtained by setting the emission wavelength from 664-850 nm and an excitation wavelength of 656 nm. Other emission spectra were taken with emission wavelengths set at 640-850 nm and an excitation wavelength at 632 nm. The second emission spectra was taken with the excitation wavelength set to that of the operating wavelength of the HeNe laser used when testing the PBGM. Emission spectra of dye **1** doped PMMA films were excited at 632 nm wavelength with an emission wavelength range of 642 – 850 nm. The excitation spectra was set over a range of 400 – 691 nm with an emission wavelength of 701 nm.

The samples were placed in a solid support apparatus at a 30° angle from the line of incidence. This was set to maximize the signal coming from solid samples.[33] The excitation and emission slit for solid samples was kept at 5 nm for all samples. A fast

Fourier transform (FFT) set to 10 points was used to reduce background noise in the spectra.

Dye samples in solution were analyzed to determine the fluorescence excitation and emission wavelengths by a Hitachi F-4500 Fluorescence Spectrophotometer (Japan). This instrument was used for solution samples because it was easily accessible at the MTSU facilities. The maximum excitation and emission wavelengths were based on the UV absorbance of the dye in solutions of $CHCl_3$. Using the same solvent, the dyes were diluted to concentrations in the 10^{-7} M region for fluorescence testing. No specific concentration was used, except for dye **8** and **1**, to find these maxima. Cy5 and dye **1** samples were created at specific concentrations to determine any correlation between fluorescence absorbance units and concentration. Excitation and emission slits were set to 5 nm for all samples in solution.

3.4.2 UV/Visible Spectroscopy

Light at certain wavelengths can excite electrons in molecules that have an appropriate electronic structure. The absorbance of energy/light excites the electrons in the molecule from the ground state to an excited state and energy of the transition can be measured by a spectrophotometer. The purpose of UV spectroscopy was to measure the maximum wavelength of absorbance of dyes **1-7** and implement the Beer Lambert Law to find the molar absorptivity (ε), also known as the molar extinction coefficient, of each dye in solution. The Beer Lambert Law is $A = \varepsilon bc$; where absorbance is A, molar absorptivity is ε, path length in cm is b, and concentration is c in mol/L.

This was done by estimating ε and solving for concentration (c) in the Beer Lambert Law, Equation 3. The path length (b) was 1 cm, and c was calculated to keep the absorbance between 0.1 and 0.8. Keeping solutions within this absorbance range insured a linear plot of concentration vs. absorbance, outside this range the absorbance of solution becomes nonlinear and the Beer Lambert Law no longer applies. The spectrophotometer used in these measurements was an Agilent Technologies diode array spectrophotometer (Santa Clara, California). The samples were tested over a wavelength range of 300-800 nm.

3.4.3 Bloch Surface Wave Analysis

The BSW's were analyzed with a HeNe laser using a Kretschmann configuration. The laser passes through a lens that allows the light to enter the prism over a range of angles. As the light travels through the prism it then passes through index matching fluid, the glass substrates upon which the multilayer was built, and the multilayer. The laser is then reflected back through the materials and into a detector or a plain white sheet of paper. This is how the mode was determined. A mode is when all light from the laser as it comes into the film is coupled with the BSW on the surface and no light is reflected back to the detector.

3.5 Polymer and Fluorescence Results and Discussion

3.5.1 UV/Vis and Fluorescence Spectroscopy

Increasing fluorescent yield through the use of photonic band gap materials and photonic crystals is a proven concept.[4,15] The mesoporous thin films can be functionalized with amine groups through the process described in Chapter II. This gave sites for the NHS

ester functionalized Cy5 dye to attach to the film. Dye **8** was initially chosen because the excitation wavelength is in the range that can be excited by the HeNe laser operating at a 632 nm wavelength. Cy5 has an excitation wavelength of 634 nm with an emission wavelength at 658 nm. While the m-SiO_2 thin films can be functionalized, the 1 % AF 1600 and 2 % PMMA can be doped with small amounts of fluorescent dye dissolved in it. The fluorescent dopant material was chosen from among several dyes synthesized in the MTSU laboratories by the Friedli research group.[31,32] These dyes along with the **8** are shown in Figure 11.

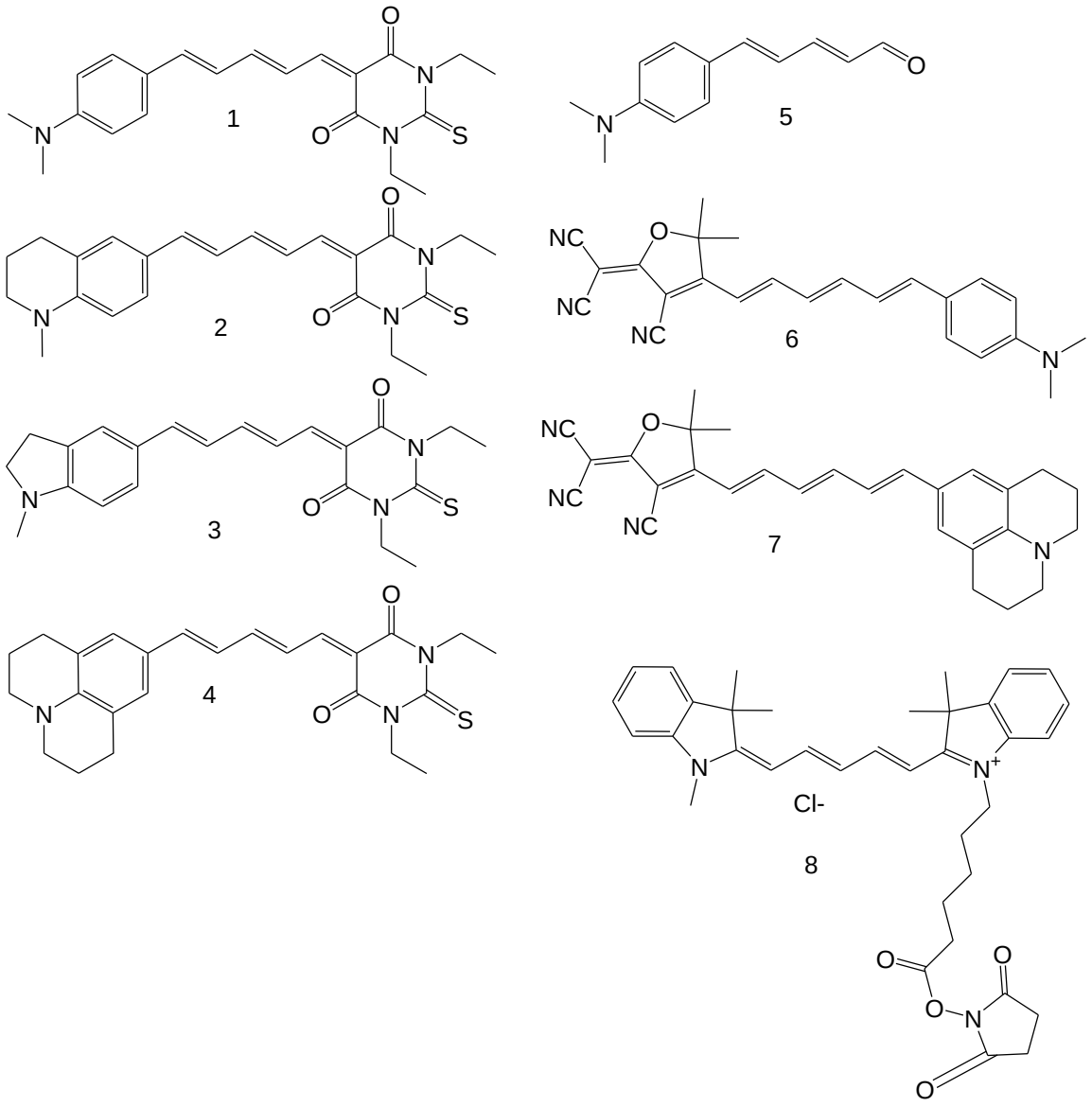

Figure 11. Structure of dyes **1-8**.

The maximum absorbance wavelengths were determined by UV/Visible spectroscopy and the molar extinction coefficients (ε) were found for dyes in solutions of chloroform. This was done by applying the Beer Lambert law in the linear absorbance region

discussed in section 3.4.2 UV/Visible Spectroscopy. Table 2 shows the maximum absorbance wavelengths and ε values.

Table 2. Maximum Absorbance Wavelength and Molar Extinction Coefficients for Donor-Pi-Acceptor Dyes **1-7** [a]

	λ_{max}	log(ε)
1	600	4.89
2	648	4.86
3	628	4.74
4	680	4.91
5	414	4.22
6	648	4.81
7	722	4.52

[a] Measured in chloroform

Determining the maximum absorbance wavelengths gave a starting point for fluorescence testing because the wavelength of maximum absorbance and excitation should be very close if not the same. Table 3 shows that dyes **1-4** are close to the range of wavelengths that can be excited by the HeNe laser. Figure 12 shows the excitation and emission spectra of dyes **1-4**, which were chosen because they gave the best fluorescence and have excitation wavelengths close to that of the HeNe laser operating wavelength. No

fluorescence was seen for dyes **6** and **7**, and dye **5** was out of wavelength range to be considered for further testing.

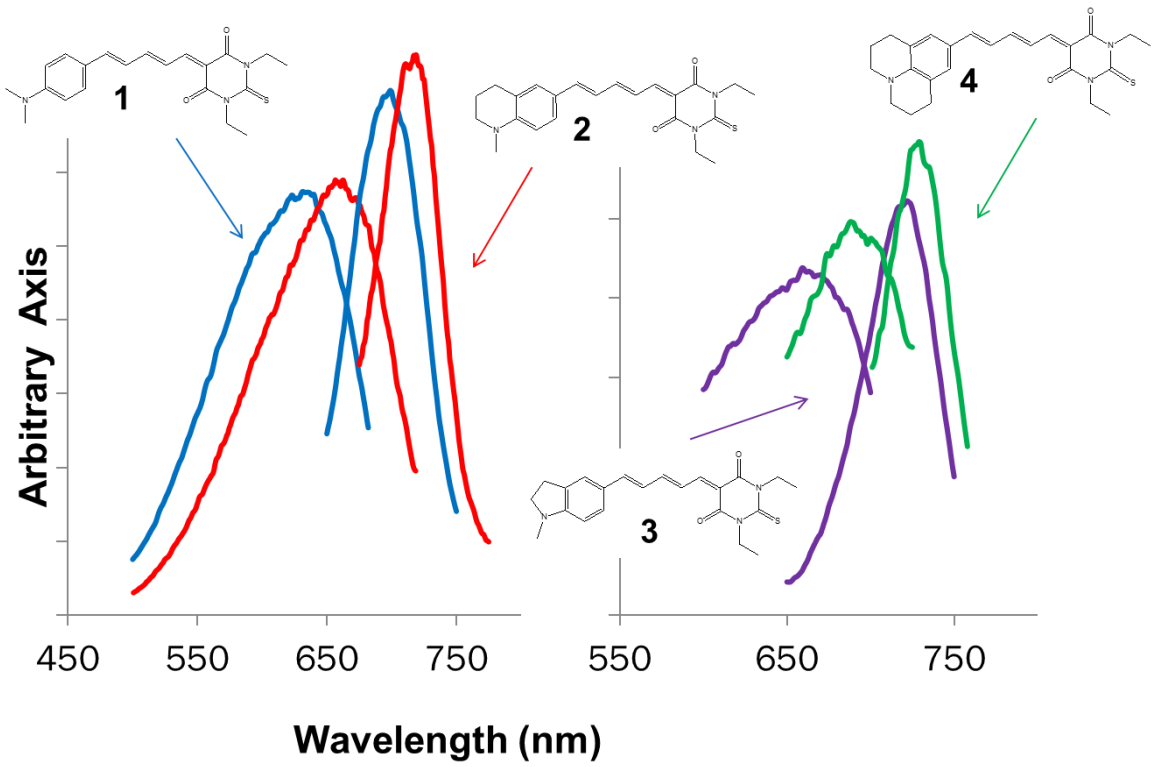

Figure 12. Excitation and emission spectra of dyes **1** (blue), **2** (red), **3** (purple), **4** (green). The color representation of the dyes is for the excitation and emission spectra shown on the same plot.

All the spectra were measured in chloroform solvent at concentrations in the 1 x10^{-7} M range. The excitation and emission wavelengths, along with Stokes shift are found in Table 3. Dye **1** was chosen as dopant because its λ_{max} (Ex) in $CHCl_3$ was determined to be the same wavelength as a HeNe laser (632 nm).

Table 3. Excitation and Emission Wavelengths (nm) of Dyes **1-4** [a]

	Excitation λ	**Emission λ**	**Stokes Shift**
1	632	696	64
2	661	671	10
3	658	721	63
4	688	728	40

[a] Measured in 1 x10^{-7} M chloroform solutions.

3.5.2 Cy 5

The Cy 5 derivatized mesoporous thin films were analyzed following the parameters mentioned earlier in this chapter (3.5.1). The λ_{max} (Ex) (634 nm) and λ_{max} (Em) (658 nm) wavelengths were as expected and the Cy5 dye could be excited with the HeNe laser in the sensing apparatus. The Stokes shift of 24 nm is very small and because no mode was given when testing the m-SiO_2 films the Cy5 derivatized films were not explored further.

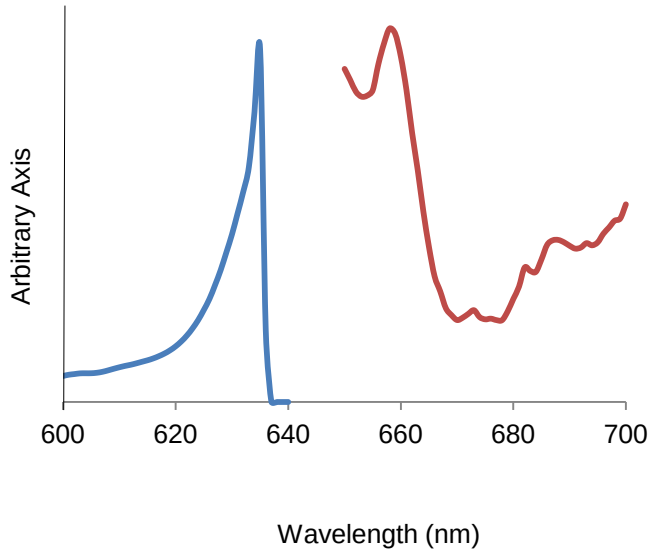

Figure 13. Cy 5 derivatized m-SiO_2 on silica substrate. Blue line represents excitation with λ_{max} (Ex) = 634 and red line represents emission λ_{max} (Em) = 658 nm.

3.5.3 AF 1600 Thin Films

An amorphous Teflon polymer, AF 1600, was chosen to replace the m-SiO_2 as the thin film on PBGM-2. Amorphous Teflon gives a large surface due to the fact that it has a high fractional free volume of 0.327 in its amorphous state.[34,35] In addition, this material was readily available and formed transparent films. Three solution concentrations of AF1600 in octofluorotoluene were made: 0.1 %, 1.0 %, and 3.0 % (w/w). The thinnest possible film can be used as a last layer to complete PBGM-2. The 0.10 % AF 1600 solution produced the thinnest film but the 1 % solution was chosen as the stock solution to use because it gave a mode when tested with the HeNe laser.

The thickness of the films created by dropping the 1 % AF 1600 solution by pipette onto the substrate was determined by profilometry. This allowed for the calculations of volume of films to be made since the area of each film was predetermined. The average thickness of these films was 4.96 μm and the area of each film was 2.28 cm^2 and from these measurements the volume of the film was found to be 1.13 x 10^{-3} cm^3.

Dye **1** was dissolved in a 1 % (w/w) AF 1600 polymer solution in octafluorotoluene (OFT). After evaporation of solvent the dye molecules were assumed to be randomly distributed in the AF 1600 films. Several concentrations were analyzed to create a calibration curve for concentration vs. fluorescence. The emission spectra were analyzed at two excitation wavelengths, 656 nm and 632 nm. The λ_{max} (Ex) for the samples was found to be 656 nm, yet 632 nm was also used because that is the wavelength the HeNe laser used in generation of BSWs. Figure 14 and 15 show the excitation and emission spectra of AF 1600 polymer films doped with dye **1**.

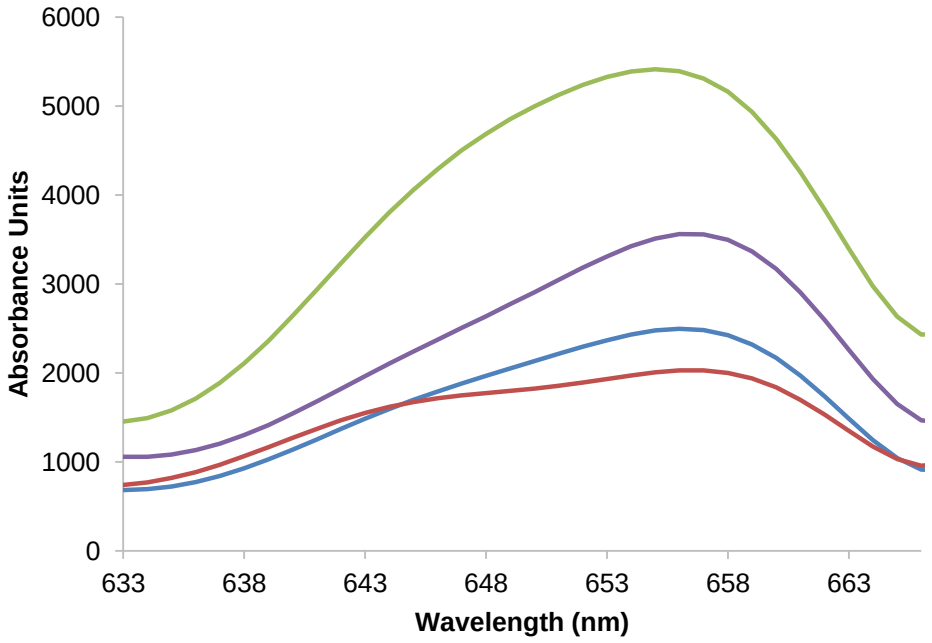

Figure 14. Excitation of four different concentrations of dye **1** in AF 1600: blue line 4.26 x 10^{-4} M with λ_{max} (Ex) = 656 nm, red line 8.53 x 10^{-4} M with λ_{max} (Ex) = 657 nm, green line 1.28 x 10^{-3} M with λ_{max} (Ex) = 655 nm, and the purple line 4.26 x 10^{-3} M with λ_{max} (Ex) = 656 nm.

Figure 14 shows the maximum excitation wavelength that is observed between 655 and 657 nm wavelengths. λmax (Ex) = 656 nm wavelength was set when scanning for the maximum emission wavelength. The scanning parameters are described earlier in this chapter and the emission spectra can be seen in Figure 15.

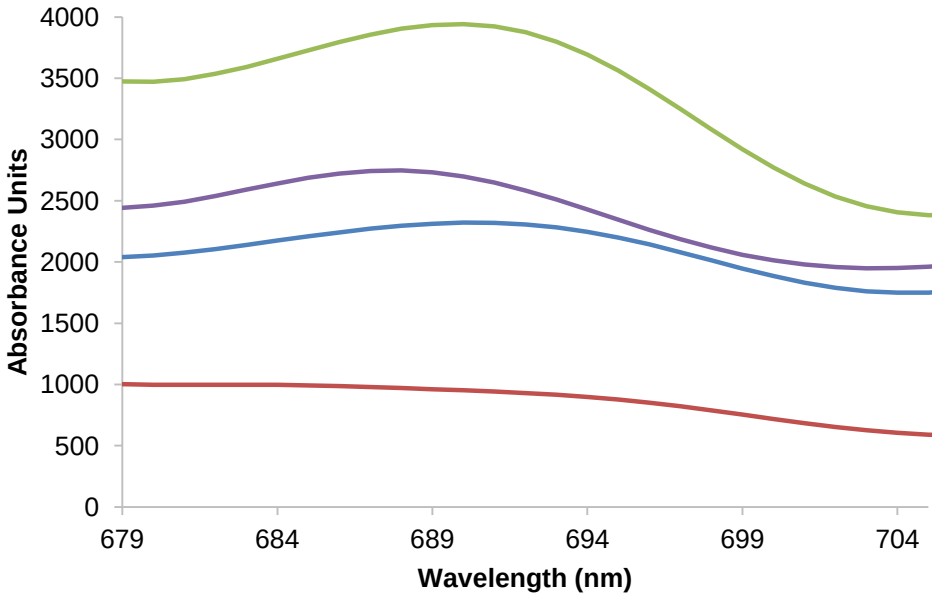

Figure 15. Emission spectra at varying concentrations of dye **1** in AF 1600 polymer with excitation wavelength set at 656 nm: blue line 4.26 x 10^{-4} M with λ_{max} (Em) = 691 nm, red line 8.53 x 10^{-4} M with λ_{max} (Em) = 683 nm, green line 1.28 x 10^{-3} M with λ_{max} (Em) = 691 nm, and the purple line 4.26 x 10^{-3} M with λ_{max} (Em) = 688 nm.

Figure 15 shows that the emission wavelength of dye **1** is from 683-691 nm. This can be compared to the spectra in Figure 16 that shows the emission spectra of dye **1** at varying concentrations when excited at 632 nm.

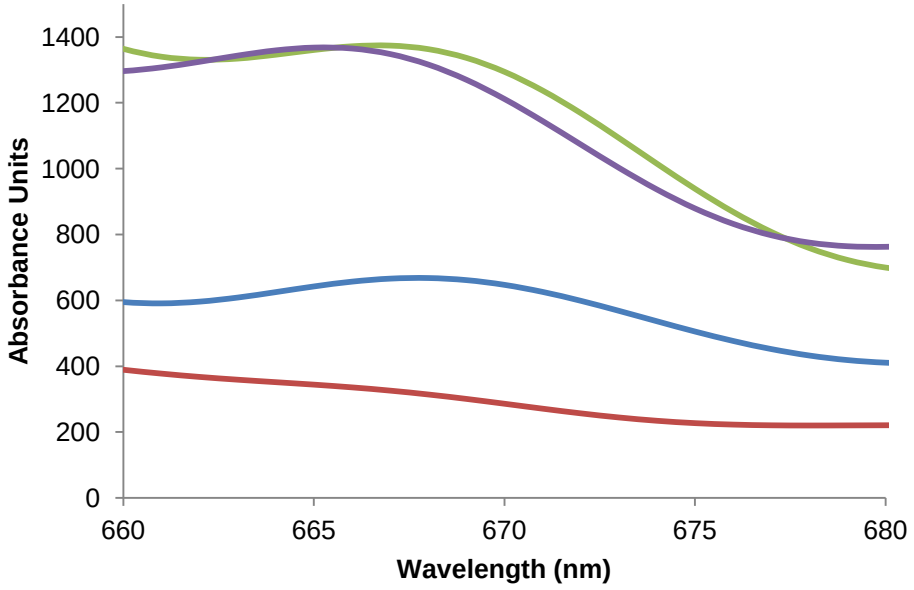

Figure 16. Emission spectra of varying concentrations of dye **1** in AF 1600 with excitation wavelength set at 632 nm: blue line 4.26 x 10^{-4} M with λ_{max} (Em) = 669 nm, red line 8.53 x 10^{-4} M with λ_{max} (Em) not calculated, green line 1.28 x 10^{-3} M with λ_{max} (Em) = 668 nm, and the purple line 4.26 x 10^{-3} M with λ_{max} (Em) = 666 nm.

Comparing Figure 15 and 16, it is noticed that the emission spectra is less intense when exciting at 632 nm than when 656 nm is used as the excitation wavelength. The emission wavelength is also shifted down to 667 nm. Even though the two spectra do not match they do prove that a HeNe laser will be able to excite dye **1** in an AF 1600 polymer film.

A calibration curve could not be prepared from the fluorescence specta due to the error in correlation of fluorescence to concentration. Figure 14 shows that lower concentrations of dye **1** have a higher fluorescent yield than that of higher concentrations. There are several possible explanations for this undesired effect. One problem that arose

was the thickness of each film was not controllable with the technique used. Pipetting the solutions onto silica plates was intended to allow films to set evenly in a defined area. The film set inside pre built silica walls but varied in thickness by ± 1 μm. With this much error in the film thickness the dye would vary in concentration by an average of M ± 1.8 x 10^{-4}. In the concentration range of films shown in Figure 15 and 16 this unpredictable concentration range contributes to a large error. Because concentration changes with the thickness of the films, a large change in film thickness will cause a large change in concentration across the film surface.

Self quenching of the dye in the polymer film is another possible cause. Molecules within close proximity can transfer energy from the excited state of one molecule to the ground state of a nearby molecule. This quenches the fluorescence emission due to the fact that the excited photons are not leaving the system. Moleculses can form aggregates in two common structural formations known as H and J aggregates. In J aggregation molecules align head to tail with their positive and negative sides interacting, and in H aggregation the molecules are stacked one on top the other. These aggregates are classified by their shift in absorption maxima with J type having a bathochromic shift (shift to higher wavelengths) and H type have a hypsochromic shift (shift to lower wavelength). While J aggregates usually fluoresce at a longer wavelength, the H aggregates show strong quenching and shift to shorter wavelengths. This has been demonstrated for a number of dimer aggregates of well known fluorophores such as fluorescein , thionine, methylene blue, and other cyanine dyes.[36] Looking at the results

for the AF 1600 films, a slight hypsochromic shift compared to dye **1** in films and strong quenching, it appears that H type aggregtes are forming in the polymer.

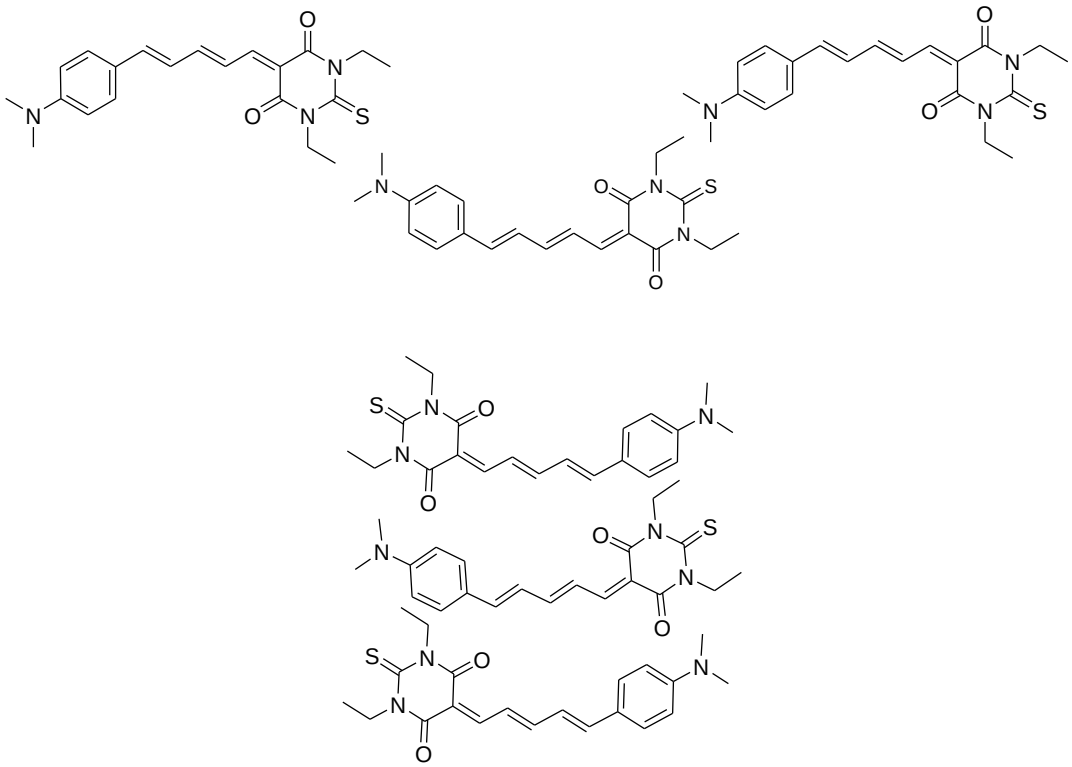

Figure 17. J aggregation (top) and H aggregation (bottom) of dye **1**

3.5.4 PMMA Thin Films

Changing the polymer thin film to an amorpohous poly(methyl methacrylate) (PMMA) polymer doped with dye **1** overcame the solvent effect and quenching problems observed in AF 1600 films. PMMA is commonly used in fluorescence sensing of dye doped polymers and is well known for its excellent optical properties. The films were made by pipetting solution onto silica plates with predetermined areas the same as AF 1600 films. With an average film thickness of 7 μm, the volume of the film was found to

be 1.37 x 10^{-3} cm^3. The solvent used in making the films and dye doped films is chloroform which was used to test the fluorescence of dyes in solutions. This gave an easy route to creating a well dissolved solution because both the polymer and dye are soluble in chloroform. Working in similar concentration ranges as the previous thin films, dye **1** doped PMMA thin films were tested. Figures 18 and 19 show the results of these tests.

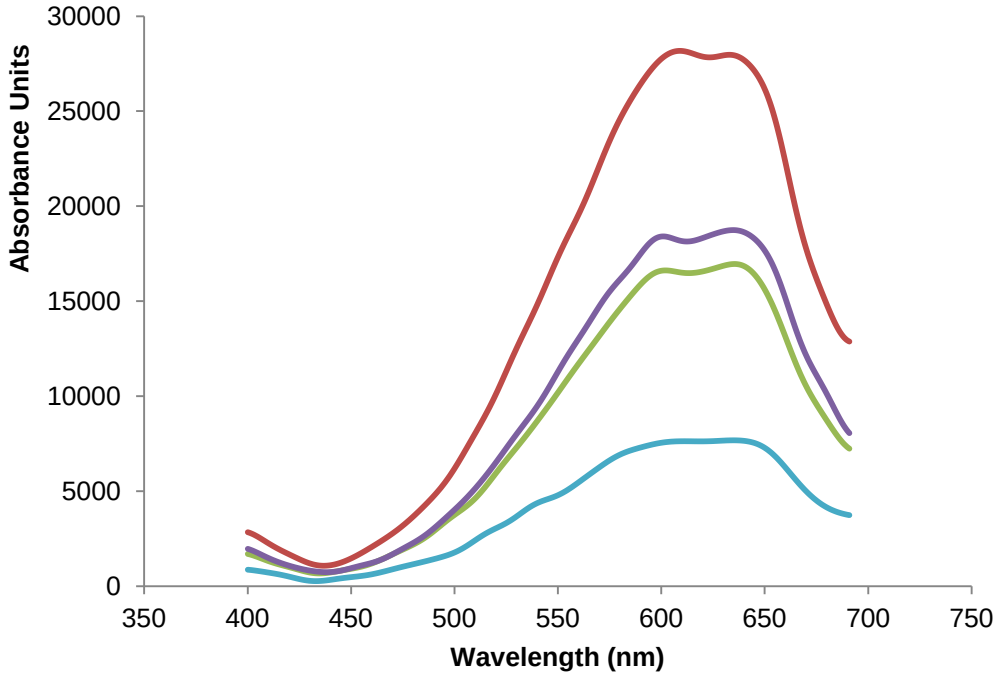

Figure 18. Excitation spectra of varying concentrations of dye **1** doped PMMA thin films: red line 1.45 x 10^{-3} M with λ_{max} (Ex) = 599 nm and 639 nm, purple line 1.11 x 10^{-3} M λ_{max} (Ex) = 601 nm and 643 nm, green line 7.26 x 10^{-4} M with λ_{max} (Ex) = 602 nm and 643 nm , and the blue line is 3.83 x 10^{-4} M with λ_{max} (Ex) = 600nm and 646 nm.

Figure 18 shows the excitation of several concentrations of dye **1** doped PMMA thin films. The maximum wavelength has double maxima at 600 nm and 645 nm. These maxima are close to 20 nm lower than λ_{max} (Ex) in the AF 1600 thin films. The 635 nm maximum is also very close to the wavelength of the HeNe laser that is used in our sensing apparatus. This is the reason for the emission testing of the PMMA thin films using the excitation wavelength of 632, since the maximum found is only 3 nm difference.

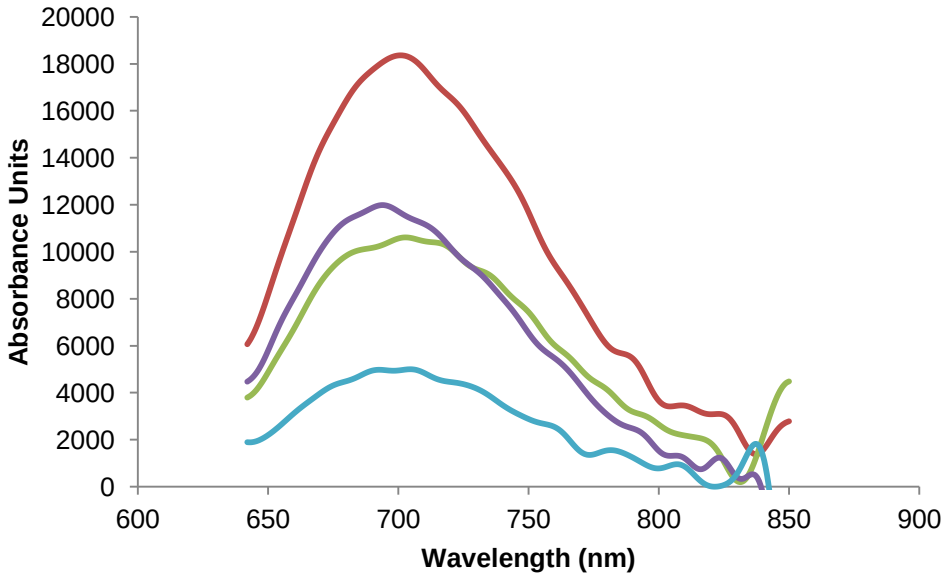

Figure 19. Emission spectra of several concentrations of dye **1** doped PMMA thin films: red line 1.45 x 10^{-3} M with λ_{max} (Em) = 703 nm, purple line 1.11 x 10^{-3} M with λ_{max} (Em) = 696 nm, green line 7.26 x 10^{-4} M with λ_{max} (Em) = 703 nm, and the blue line is 3.83 x 10^{-4} M with λ_{max} (Em) = 705 nm.

Figure 19 shows that the maximum excitation wavelength is around 700 nm. This is increases from the previous 686-689 nm maxima of the AF 1600 thin films. The Stokes shift increasses from around 30 nm to close to 70 nm. This will help in the sensing device due to the fact that the Stokes shift is increased. With a small Stokes shift, the sensing apparatus will need to filter out the excited light to focus on the emission wavelengths.

Although the 2% PMMA films gave better spectra than the AF 1600 thin films; the thickness of the films pipetted on the to the substrate along with the varying size of the films gives an error value too large for precise measurements. If the size of the film varies by ± 1 mm and the film thickness varies ± 1 μm then the concentrations of each film would change due to volume changes and these calculations are shown in the following figure.

Table 4. Calculated Error Values for Dye Concentration in PMMA Films

Concentration M[a]	**Concentration M(+)**[b]	**Concentration M(-)**[c]	**Standard Deviation**	**95 % Confidence**
1.45×10^3	1.0×10^3	2.02×10^3	4.68×10^4	5.29×10^4
1.11×10^3	8.3×10^4	1.54×10^3	3.57×10^4	4.04×10^4
7.26×10^4	5.45×10^4	1.01×10^3	2.34×10^4	2.65×10^4
3.83×10^4	2.87×10^4	5.32×10^4	1.23×10^4	1.39×10^4
			Avg. 95% =	3.34×10^4

[a]Calculated concentration of film based on average thickness
[b]Calculated concentration: + 1 mm in both length and width of base; + 1 μm thickness
[c]Calculated concentration: - 1 mm in both length and width of base; - 1 μm thickness

The average change in film concentration is M ± 3.34 x 10^4 for the films with spectra shown in Figures 18 and 19. These error values were too large to continue prepping samples in this way. Using the same sample solutions but spin-coating the samples onto silica plates and testing the fluorescence was proven to work better than pipetting the films into predetermined rectangular areas. Spin-coating the dye doped 2 % PMMA films gave much better results compared to that of the pipetted films. Figure 20 and 21 show the excitation and emission spectra of these films.

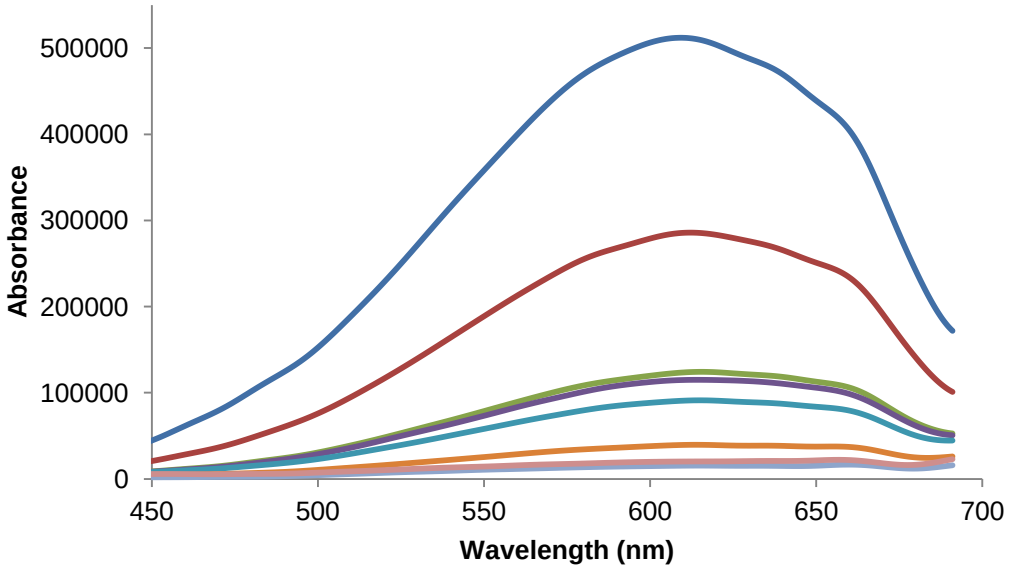

Figure 20. Excitation spectra of spin-coated dye **1** doped 2% PMMA thin films. Concentrations in descending order: 2.65 x 10^{-2} M with λ_{max} (Ex) = 609 nm, 1.32 x 10^{-2} M with λ_{max} (Ex) = 612 nm, 5.27 x 10^{-3} M with λ_{max} (Ex) = 615 nm, 4.00 x 10^{-3} M with λ_{max} (Ex) = 616 nm, 2.67 x 10^{-3} M with λ_{max} (Ex) = 615 nm, 1.33 x 10^{-3} M with λ_{max} (Ex) = 615 nm, 4.22 x 10^{-4} M λ_{max} (Ex) not observed, 5.62 x 10^{-4} M with λ_{max} (Ex) not observed.

Figure 20 shows that absorbance values correlate with concentration except for the lowest concentrations. This was not seen with the pipetted films. The λ_{max} (Ex) changed form the two points shown in figure 18 near 600 and 645 nm to just one point near 615 nm. With the decrease in pathlength, the maximum wavelength shifts accordingly. The average thickness of the spin-coated films was 224 nm ± 11 nm (determined by ellipsomtry). Figure 21 shows the same correlation for emission wavelengths.

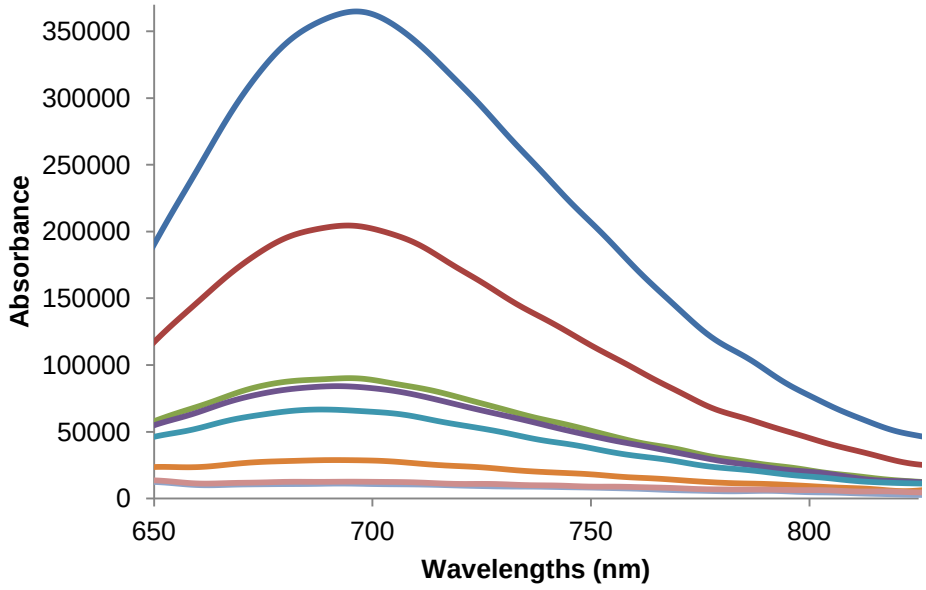

Figure 21. Emission spectra of spin-coated dye **1** doped 2% PMMA thin films. Concentrations in descending order: 2.65 x 10^{-2} M with λ_{max} (Em) = 696 nm, 1.32 x 10^{-2} M with λ_{max} (Em) = 695 nm, 5.27 x 10^{-3} M with λ_{max} (Em) = 695 nm, 4.00 x 10^{-3} M with λ_{max} (Em) = 692 nm , 2.67 x 10^{-3} M with λ_{max} (Em) = 689 nm, 1.33 x 10^{-3} M with λ_{max} (Em) = 692 nm, 4.22 x 10^{-4} M λ_{max} (Em) not observed, 5.62 x 10^{-4} M λ_{max} (Em) not observed.

The emission spectra were taken with an excitation wavelength of 610 nm because this was determined to be the λ_{max} (Em). Slit openings, incriments, and

smoothing are same for all spectra. Figure 21 shows that the change in film thickness alters the emission maximum wavelength from 700 nm for the pipetted films in Figure 19 to 695 nm for the spin-coated films. The change in film thickness is from 7 um (pipetted film) to 224 nm ± 11 nm (spin-coated films). With the change in the excitation and emission wavelengths another plot of concentration dependence on fluorescence was generated with the spin-coated films excited at 632 nm (HeNe laser). This plot is shown in the following figure, Figure 22.

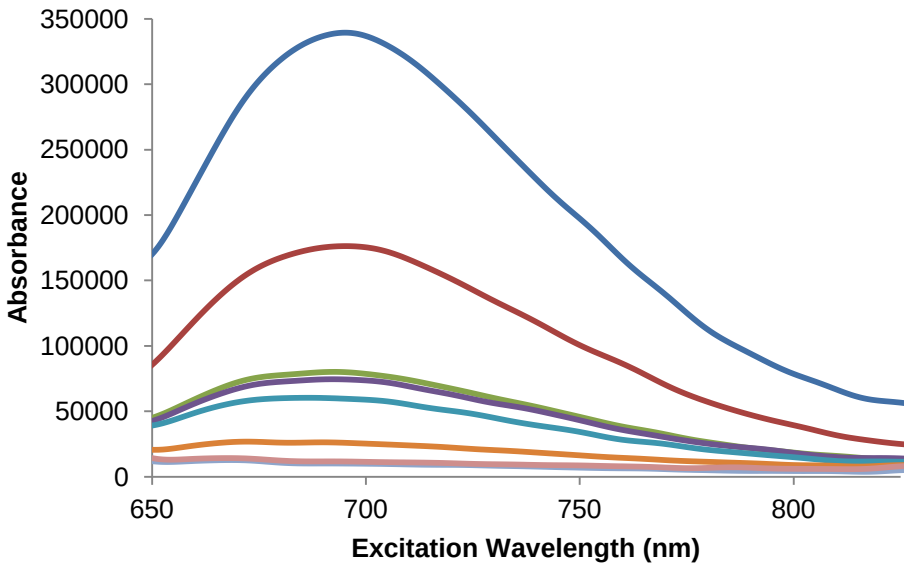

Figure 22. Emission spectra of dye **1** doped 2% PMMA thin film excited at 632 nm. Concentrations in descending order: 2.65 x 10^{-2} M with λ_{max} (Em) = 695 nm, 1.32 x 10^{-2} M with λ_{max} (Em) = 695 nm, 5.27 x 10^{-3} M with λ_{max} (Em) = 693 nm, 4.00 x 10^{-3} M with λ_{max} (Em) = 692 nm, 2.67 x 10^{-3} M with λ_{max} (Em) = 687 nm, 1.33 x 10^{-3} M with λ_{max} (Em) = 690 nm, 4.22 x 10^{-4} M with λ_{max} (Em) not observed, 5.62 x 10^{-4} M with λ_{max} (Em) not observed.

The emission wavelengths appear to be in the same region compared to the emission spectra taken at an excitation wavelength of 610 nm and shows that the thin films will excite when in contact with the HeNe laser.

To compare fluorescence results from batches of films, the overlayed spectra are shown in Figure 23.

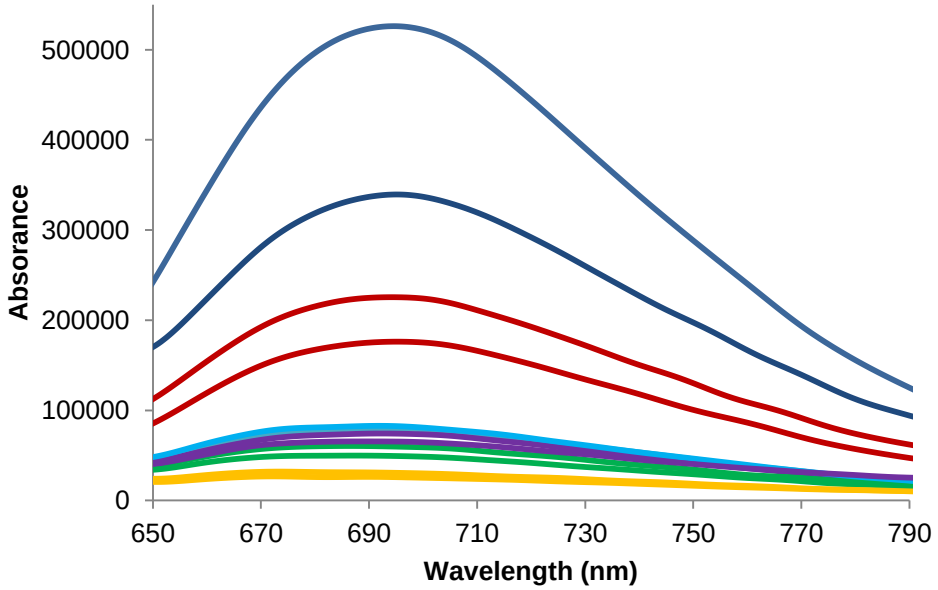

Figure 23. Emission spectra comparing two sets of data excited at 632 nm. Concentrations in descending order: 2.65 x 10^{-2} M, 1.32 x 10^{-2} M, 5.27 x 10^{-3} M, 4.00 x 10^{-3} M, 2.67 x 10^{-3} M, 1.33 x 10^{-3} M.

The percent change in the spectra was calculated by finding the maximum absorbance from each spectrum and comparing it to spectra from the thin film with the same concentration. These calculations gave an average percent change of 18.6 % ± 9.5 %

which is better than the thicker films. Each set of data was plotted to show the linear correlation of emission maxima versus concentration and is shown in Figure 24. Figure 24 shows the linear regression between emission maxima and concentration for two sets of data made from the same batch of materials. The maximum fluorescence emission from one batch to the next changes enough to give two obviously different linear regression lines (red and green dotted lines). Even though the same concentration of dye **1** was in each film, varying emission values did not allow for a standard linear calibration. As seen by the error bar values, it is also apparent that the more concentrated samples had more error than the less concentrated ones.

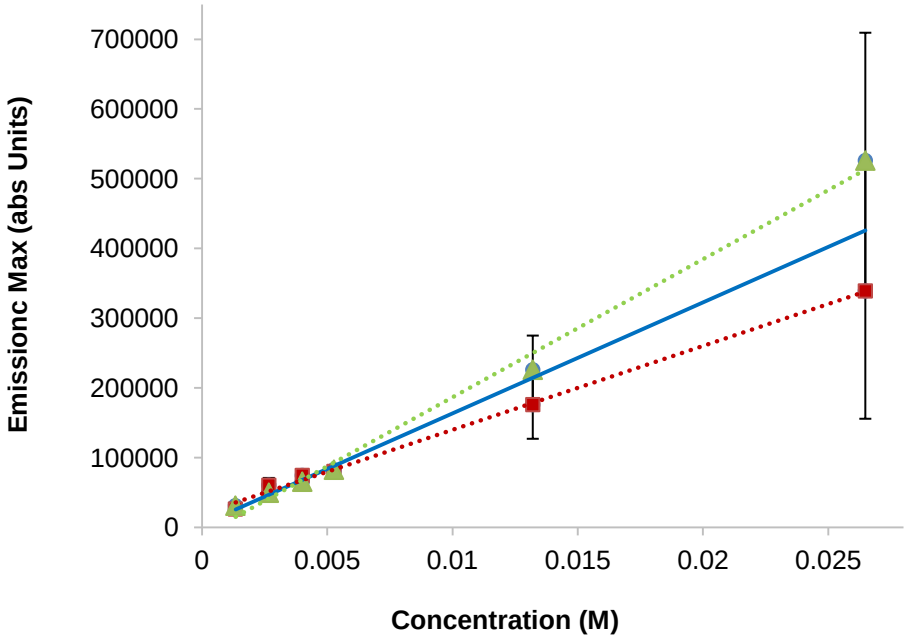

Figure 24. Linear calibration of emission versus concentration of dye **1** doped PMMA films. Green dotted line linear regresion: $y = 2 \times 10^7 x - 11313$ with $R^2 = 0.9935$. Red dotted line linear regression: $y = 1 \times 10^7 x + 19918$ with $R^2 = 0.9967$. The blue line represents a linear regression between all data points from both batches with linear regression of $y = 2 \times 10^7 x + 4302.3$ with $R^2 = .9227$. The error bar values are the confidence interval between the two data points with same concentration.

The next step in fluorescence testing is to apply the dye doped polymer to the PBGM and see if it produces an increase in fluorescence yield by coupling the HeNe laser to BSW generated by the PBGM. For comparison, the same test should be run with the dye-doped polymer applied to a regular glass slide.

CHAPTER IV

GRATING

4.1 Grating Formation

Researchers in the MTSU Physics Department are currently working on a model for a grating that can be used as a waveguide for TiO_2/SiO_2 PBGMs. While this was being done a proof-of-concept experiment was done on polymer and m-SiO_2 materials using a stamp available in the Weiss research group at Vanderbilt University. The reusable stamp was patterned by traditional lithography and reactive ion etching with a specific grating pattern. Such stamps can be applied to films using the direct imprinting of porous surfaces (DIPS) technique[20] under pressure at room temperature in a short and easy process. The reusable stamp also takes away the need of any further etching, curing or baking of the sample.[4] A hydraulic press was used to press the stamp in some of the thin films reported here: m-SiO_2 thin films at 140 psi; AF 1600 thin films at 100 psi. Thin films were then analyzed by SEM to determine the quality and dimensions of the resulting grating.

4.2 Results and Discussion

DIPS allows for an easier experimental set up when testing the reflectance change in the PBGM material.[20] A hydraulic press was used to press the stamp into the thin films. Starting at a moderate pressure of 80 psi, to avoid cracking the stamp or substrate, the press pushed the stamp pattern into the film. After checking the grating under a microscope, the process was done again at a higher pressure to make sure the stamp pressed fully into the material. The m-SiO_2 on silica plates tolerated up to 140 psi

to stamp the grating into the film. On PBGM-2 however, 120 psi was applied to the stamp and cracked the sample due to the fact that PBGM-2 is deposited on a glass slide and is also a thinner film than those on silica plates. The 1% AF 1600 films were stamped at 100 psi and this pressure worked for both silicon wafer and PBGM substrates. The AF 1600 copolymer is much softer than m-SiO_2, therefore requires lower pressures for successful transfer of patterns via DIPS.

When the right grating is applied, the HeNe laser will couple with the BSW on the surface of the PBGM without the use of a prism. Figure 25 A shows a single grating that is part of a stamp that contains twelve (3 rows of 4 each) different grating areas (Figure 25 B).

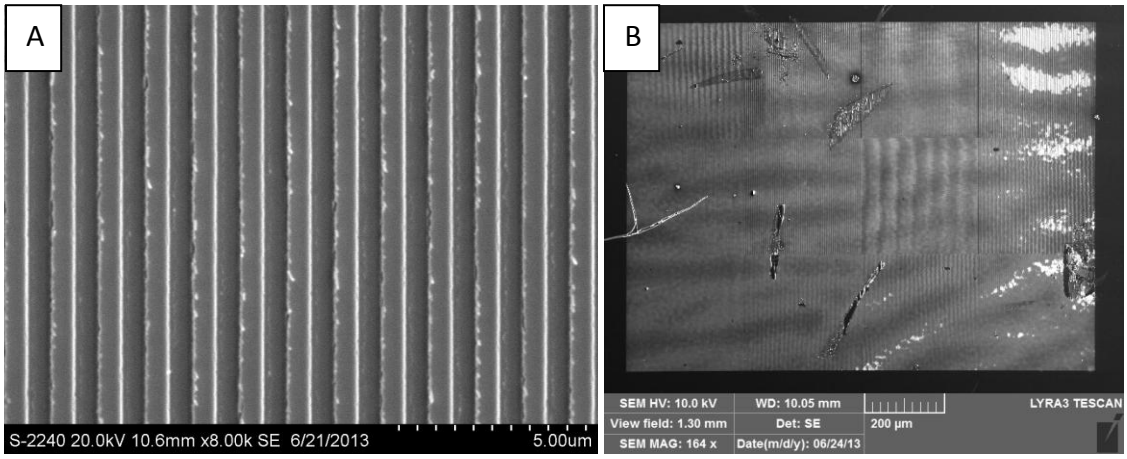

Figure 25. SEM images of a 120 µm grating on a m-SiO_2 thin film showing only one grating out of twelve (left), and B) SEM image of all gratings of the stamp used on AF 1600 thin film (right). Images taken by Joyce Miller of MTSU Interdisciplinary Microanalysis and Imaging Center (MIMIC)

The SEM images show that the DIPS process works on both m-SiO_2 and AF 1600 thin films. The image taken of the m-SiO_2 stamped material shows only one of the 12 gratings. This is due to the fact that the m-SiO_2 is inorganic and more resistant than the AF 1600 organic polymer to the high energy of the electron beam of the SEM allowing for a closer view of the sample. The SEM image in Figure 8B was taken using a focused ion beam (FIB) microscope. The image was taken at lower magnification so that the ion beam did not destroy the sample. The exact grating dimensions needed to guide light into these materials has yet to be determined, but the simplicity and success of the DIPS process has been demonstrated.

CHAPTER V

CONCLUSIONS

Alternating SiO_2/TiO_2 PBGMs with the outer SiO_2 layer missing or present in half the required thickness were used to investigate fluorescence enhancement *inside* porous thin films. Three thin films were examined. First, m-SiO_2 was spin-coated into ~750 nm thick films with a hexagonal morphology from an established sol-gel recipe. Because a mode indicating BSW coupling was not observed from films processed on PBGM-1, the sol-gel recipe was modified to produce m-SiO_2 films with hexagonal morphology of a thickness of ~1 μm in order to provide a film with refractive index closer to the missing SiO_2 layer. Surprisingly, this thicker film on PBGM-1 also did not produce a mode. Because of the difficulties encountered in obtaining good quality ~1 μm thick m-SiO_2 films, the PBGM multilayer design was changed to maximize the BSW electric field closer to the surface of the PBGM, theoretically requiring a thinner m-SiO_2 film. Heat-induced peeling of the PBGM layer required a decrease in calcification temperature from 600 ^{o}C to 200 ^{o}C, followed by methanol extraction to produce films with good optical quality. Dilution of the sol-gel recipe to produce a thinner m-SiO_2 film also changed the morphology to wormlike, but these films were reproducible with a typical thickness of 324 nm with good optical quality and an average pore diameter of 7 nm. Unfortunately, no mode has been observed for any m-SiO_2 films to date on PBGM-2.

Although the m-SiO_2 films did not appear to couple with BSWs regardless of film thickness and PBGM design, Cy5 dye was coupled to the surface through a reactive NHS

linker. Although the overlap between HeNe excitation (632 nm) and λ_{max} of Cy5 in m-SiO_2 (750 nm) was acceptable, the Stokes shift between excitation and emission for Cy5 was only 24 nm (Figure 13), which is quite small for the determination of fluorescence enhancement.

Therefore, a more suitable dye was chosen from the series of donor-pi-acceptor dyes **1-7**. Since dyes **1-4** fluoresced in a region that can be excited by a HeNe laser, dye **1** with ICT λ_{max} (Ex) that best overlapped with the HeNe excitation wavelength, and gave a good Stokes shift (Figure 12) was used.

Next, organic polymer thin films were tested as host materials for dye **1** to ensure coupling to BSWs to give a mode. Fluorinated copolymer AF 1600 was investigated first because it is known to be particularly porous and had produced a mode as a spin-coated film on PBGM-1. Both dye **1** and 1% w/w AF 1600 copolymer were soluble in octofluorotoluene solvent. The dye-doped organic polymer was applied to silicon wafers as ~5 μm thick films with a 4 $x10^{-3}$- 4 $x10^{-4}$ M range of dye concentrations to obtain a calibration curve of fluorescence intensity versus concentration. The error in determination of concentration was large due to variations in thickness across the films. Dye fluorescence was almost completely quenched in AF1600 over the entire concentration range. This is best explained by H-aggregation, in which polar molecules line up with donor end overlapping with acceptor end of the molecule accompanied by a hypsochromic shift and quenching (Figure 15 and 16).

PMMA films, cast from 2% w/w solutions in chloroform, had the best optical quality, thicknesses of ~224 nm, and no evidence of dye aggregation. A linear calibration curve for dye fluorescence was observed over a range of a 10^{-2}-10^{-4} M, although error between independently prepared batches increased markedly as concentration increased (Figure 24). The minimum detection limit for fluorescence in 224 ± 11 nm thick films was 1.33 x 10^{-3} M. The ± 11nm is error based off ellipsometer readings taken to determine thickness of PMMA films, and the λmax (Em) error associated with this limit is ± 16%.

The minimum observed fluorescence enhancement for SPs is 11%.[3] Since spectroscopic enhancements have been reported to be as high as 16 times for Au[2] and sensitivity of BSW mode shifts on PBGM slides were estimated to be 30 times that of fluorescence microscopy,[7] the error is expected to be small compared to the enhancement.

Another direct investigation of BSW coupling with dye **1** evaporated from solvent onto PBGM-2 surface will be performed. This will be done by spin-coating the dye from solution onto the PBGM-2 with no polymer added. With the small amounts of dye molecules spread across PBGM-2 a shift in the mode is expected to be observed.

Finally, a proof of principle demonstrating that a gradient can be applied to m-SiO_2 or polymer surfaces was successful. The DIPS process used in this research worked well enough to make a grating specific to PBGM-2 for further testing.

Work Cited

1. LeRu, E. C.; Blackie, E.; Meyer, M. Etchegoin, P. G. Surface Enhanced Raman Scattering Enhancement Factors: A Comprehensive Study. *J. Phys. Chem.* **2007**, *111*, 13794-13803.
2. Liebermann, T.; Knoll, W. Surface-Plasmon Field-Enhanced Fluorescence Spectroscopy. *Colloid. Surface. A.* **2000**, *171*, 115-130.
3. Neal, T. D.; Okamoto, K.; Scherer, A. Surface Plasmon Enhanced Emission From Dye Doped Polymer Layers. *OSA PROC.* **2005**, *13*, 5522-5527.
4. Gao, J.; Sarangan, A. M.; Zhan, Q. Experimental Confirmation of Strong Fluorescence Enhancement Using One-Dimensional GaP/SiO_2 Photonic Band Gap Structure. *Opt. Mater. Express* **2011**, *1*, 1216-1223.
5. Shinn, M.; Robertson, W. M. Surface Plasmon-like Sensor Based on Surface Electromagnetic Waves in a Photonic Band Gap Material. *Sensor. Actuat. B-Chem.* **2004**, *105*, 360-364.
6. Farmer, A. F.; Friedli, A. C.; Wright, S. M.; Robertson, W. M. Biosensing Using Surface Electromagnetic Waves in Photonic Band Gap Multilayers. *Sensor. Actuat. B-Chem.* **2012**, *173*, 79-84.
7. Friedli, A. C.; Wright, S. M.; Robertson, W. M. Biosensor Research: SERRI Phase I and II Final Reports, Oak Ridge National Laboratory. August **2010,** December **2011**. http://www.serri.org/publications/Pages/Reports.aspx
8. *An introduction to Fluorescence* Spectroscopy. Perkin Elmer. **2000.**

9. Brandt, M. Fluorescence Spectroscopy. Rose-Hulman Institute of Technology. **2010**, 20-37. http://www.rose-hulman.edu/~brandt/Fluorescence/Quenching_processes.pdf (accessed February 17, 2014).
10. Chen, L.; McBranch, D. W.; Wang, H.; Helgeson, R.; Wudl, F.; Whitten, D. G. Highly Sensitive Biological and Chemical Sensors Bases on Reversible Fluorescence Quenching in a Conjugated Polymer. *P. Natl. Acad. Sci.-Biol*. **1999**, *96*, 12287-12292.
11. Toal, S. J.; Trogler, W. C. Polymer Sensors for Nitroaromatic Explosives Detection. *J. Mater. Chem.* ***2006***, *16*, 2871-2883.
12. Vu, A.; Phillips, J.; Buhlmann, P.; Stein, A. Quenching Performance of Surfactant-Containing and Surfactant-Free Fluorophore-Doped Mesoporous Silica Films for Nitroaromatic Compound Detection. *Chem. Mater*. **2013**, *25*, 711-722.
13. Barnes, W. L.; Dereux, A.; Ebbesen, T. W. Surface Plasmon Subwavelength Optics. *Nature*. **2003**, 424, 824-830.
14. Soboleva, I. V.; Descrovi, E.; Summonte, C.; Fedyanin, A. A.; Giorgis, F. Fluorescence Emission Enhanced by Surface Electromagnetic Waves in One-Dimensional Photonic Crystals. *Appl. Phys. Lett.* **2009**, *94*, 231122-1-231122-3.
15. Zhang, Y.; Wang, J.; Ji, Z.; Hu, W.; Jiang, L.; Song, Y.; Zhu, D. Solid-State Fluorescence Enhancement of Organic Dyes by Photonic Crystals. *J. Mater. Chem*. **2007**, *17*, 90-94.

16. Ballarini, M.; Frascella, F.; Michelotti, F.; Digregario, G.; Rivolo, P.; Peader, V.; Musi, F.; Giorgis, F.; Descrovi, E. Bloch Surface Waves-Controlled Emission of Organic Dyes Grafted on a One-Dimensional Photonic Crystal. *Appl. Phys. Lett*. **2011**, *99*, 043302-1 – 043302-3.
17. Liscidini, M.; Sipe, J. E.; Enhancement of Diffreaction for Biosensing Applications via Bloch Surface Waves. *Appl. Phys. Lett*. **2007**, *91*, 253125-1 -253125-3.
18. Giorgis, F.; Descrovi, E.; Summonte, C.; Dominici, L.; Michelotti, F. Experimental Determination of the Sensitivity of Bloch Surface Waves Based Sensors. *Opt. Mater. Express*. **2010**, *18*, 8087-8093.
19. Michl, J.; Thulstrup, E. W. *Spectroscopy with Polarized Light; Solute Alignment by Photoselection, in Liquid Crystals, Polymers, and Membranes*. VCH Publisher, Inc.: New York, **1986**.
20. Ryckman, J. D.; Liscidini, M; Sipe, J. E.; Weiss, S. M. Direct Imprinting of Porous Substrates: A Rapid and Low-cost Approach for Patterning Porous Nanomaterials. *Nano Lett*. **2011,** *11*, 1857-1862.
21. Ballarini, M.; Frascella, F.; Enrico, E.; Madracci, P.; De Leo, N.; Mechelotti, F.; Giorgis, F.; Descrovi, E. Bloch Surface Waves-Controlled Fluorescence Emission: Coupling into Nanometer-Sized Polymeric Waveguides. *Appl. Phys. Lett.* **2012**, *100*, 063305-1 – 063305-4.
22. Scott, B. J.; Wirnsberger, G.; Stucky, G. D. Mesoporous and Mesostructured Materials for Optical Applications. *Chem. Mater*. **2001**, *13*, 3140-3150.

23. Wirnsberger, G; Scott, B. J.; Stucky, G. D. pH Sensing with Mesoporous Thin Films. *Chem Commun.* **2001**, 119-120.

24. Caipa Campos, M. A.; Trilling, A. K.; Yang, M.; Giesbers, M.; Beekwilder, J.; Paulusse, J. M. J.; Zuilhof, H. Self-Assembled Functional Organic Monolayers on Oxide-Free Copper. *Langmuir* **2011**, *27*, 8126-8133.

25. Nobel Prize. The Transmission Electron Microscope. http://www.nobelprize.org/educational/physics/microscopes/tem/ (Accessed October 8, 2013)

26. Australian Microscopy and Microanalysis Research Facility. Background Information – What is Transmission Electron Microscopy? http://www.ammrf.org.au/myscope/tem/background/ (Accessed October 8, 2013)

27. ImageJ: Image Processing and Analysis in Java. http://rsbweb.nih.gov/ij/index.html (Accessed October 8, 2013)

28. KLA Tencor. P-16+ Surface Profilers. http://www.kla-tencor.cn/en/products/p-16 (Accessed on October 11, 2013)

29. A Short Course in Ellipsometry. *Guide to Using WVASE32® Software for Spectroscopic Ellipsometry Data Acquisition and Analysis*; WexTech Systems, Inc.: New York, **2001**, *3*.335, 2-1 – 2-26

30. Yang, C; Fan, H; Qui, S; Xi, Y; Chen, J. Effects of Thermal Expansion Coefficient Mismatch on Structure and Electrical Properties of TiO_2 Film Deposited on Si Substrates. *Surf Rev Lett*. **2008**, *15*, 487-491.

31. Greco, P. F. D. A. Part I. Synthesis and Characterization of Donor-pi-Acceptor Compounds with Pentedienyl-Bridged Indoline and Tetrahydroquinoline Donors and Aldehyde and Thibarbituric Acid Acceptors PartII. Longitudinal Study Comparing Online Versus Face-to-Face Course Delivery in Introduction Chemistry. Dissertation, Middle Tennessee State University, **2012.**
32. Friedli, A. C.; Robinson, M. A.; Greco, P. F.; Gonzalez, H. J.; Gootee, A. J. Effect of Pyramidalization at Nitrogen in a Series of Donor-Pi-Acceptor Dyes. 246th ACS National Meeting, Indianapolis, IN, September 8-12, 2013; American Chemical Society: Washington DC, **2013**; ORGN-563.
33. Personal communication with Dmitry Koktysh lab supervisor, VINSE Nanocrystal Fabrication Laboratories.
34. Pinnau, I.; Toy, L. G. Gas and Vapor Transport Properties of Amorphous Perfluorinated Copolymer Membranes Based on 2, 2-Bistrifluoromethyl-4, 5-Difluoro-1, 3Dioxole/tetrafluoroethylene. *J. Membrane Sci*. **1996**, *109*, 125-133.
35. Zhao, H.; Zhang, J.; Wu, N.; Zhang, X.; Crowley, K.; Weber, S. G. Transport of Organic Solutes Through Amorphous Teflon AF Films. *J. Am. Chem. Soc.* **2005**, *125*, 15112-15119.
36. Rosch, U.; Yao, S.; Wortmann, R.; Wurthner, F. Fluorescent H-Aggregates of Merocyanine Dyes. *Angew. Chem. Int*. **2006**, *24*, 7026-7030